

The NCA-1 and NCA-2 ion channels function downstream of G_q and Rho to regulate locomotion in *C. elegans*

Irini Topalidou^{*}, Pin-An Chen[†], Kirsten Cooper^{*,1}, Shigeki Watanabe^{†,2},
Erik M. Jorgensen[†], Michael Ailion^{*}

^{*}Department of Biochemistry, University of Washington, Seattle, WA 98195

[†]Howard Hughes Medical Institute, Department of Biology, University of Utah, Salt Lake City, UT
84112

¹Current Address: Fred Hutchinson Cancer Research Center, Seattle, WA 98109

²Current Address: Department of Cell Biology, Johns Hopkins University, Baltimore, MD 21205

16 Running Title: Gq signaling activates NCA channels through Rho

17

18 key words: G_q signaling, Rho small GTPase, NCA/NALCN ion channels, *C. elegans*, G protein

19

20 Corresponding author:

21 Michael Ailion

22 Department of Biochemistry

23 University of Washington

24 Box 357350

25 1705 NE Pacific St

26 Seattle, WA 98195

27 Phone: 206-685-0111

28 email: mailion@uw.edu

29

Abstract

The heterotrimeric G protein G_q positively regulates neuronal activity and synaptic transmission. Previously, the Rho guanine nucleotide exchange factor Trio was identified as a direct effector of G_q that acts in parallel to the canonical G_q effector phospholipase C. Here we examine how Trio and Rho act to stimulate neuronal activity downstream of G_q in the nematode *Caenorhabditis elegans*. Through two forward genetic screens, we identify the cation channels NCA-1 and NCA-2, orthologs of mammalian NALCN, as downstream targets of the G_q /Rho pathway. By performing genetic epistasis analysis using dominant activating mutations and recessive loss-of-function mutations in the members of this pathway, we show that NCA-1 and NCA-2 act downstream of G_q in a linear pathway. Through cell-specific rescue experiments, we show that function of these channels in head acetylcholine neurons is sufficient for normal locomotion in *C. elegans*. Our results suggest that NCA-1 and NCA-2 are physiologically relevant targets of neuronal G_q -Rho signaling in *C. elegans*.

Introduction

Heterotrimeric G protein pathways play central roles in altering neuronal activity and synaptic transmission in response to experience or changes in the environment. G_q is one of the four types of heterotrimeric G proteins alpha subunits in animals (Wilkie *et al.* 1992) and is widely expressed in the mammalian brain (Wilkie *et al.* 1991) where it typically acts to stimulate neuronal activity and synaptic transmission (Krause *et al.* 2002; Gamper *et al.* 2004; Coulon *et al.* 2010). These roles are conserved in the nematode *C. elegans*. Unlike mammals which have four members of the G_q family, *C. elegans* has only a single $G_q\alpha$ (Brundage *et al.* 1996). In *C. elegans*, loss-of-function and gain-of-function mutants in the single $G_q\alpha$ gene *egl-30* are viable but have strong neuronal phenotypes, affecting locomotion, egg-laying, and sensory behaviors (Brundage *et al.* 1996; Lackner *et al.* 1999; Bastiani *et al.* 2003; Matsuki *et al.* 2006; Esposito *et al.* 2010; Adachi *et al.* 2010). We aim to identify the signal transduction pathways and downstream targets by which G_q signaling alters neuronal activity.

In the canonical G_q pathway, G_q activates phospholipase $C\beta$ (PLC) to cleave the lipid phosphatidylinositol 4,5,-bisphosphate (PIP2) into diacylglycerol (DAG) and inositol trisphosphate (IP3), each of which can act as a second messenger. This pathway operates in both worms and mammals, but in both systems, a number of PLC-independent effects of G_q have been described, indicating the existence of additional G_q signal transduction pathways (Lackner *et al.* 1999; Miller *et al.* 1999; Vogt *et al.* 2003; Bastiani *et al.* 2003; Sánchez-Fernández *et al.* 2014). Using a genetic screen for suppressors of activated G_q , we identified the Rho guanine nucleotide exchange factor (GEF) Trio as a direct effector of G_q in a second major G_q signal transduction pathway independent of the canonical PLC pathway (Williams *et al.* 2007). Biochemical and structural studies demonstrated that G_q directly binds and activates RhoGEF proteins in both worms and mammals, indicating that this new G_q pathway is conserved (Lutz *et al.* 2005, 2007; Williams *et al.* 2007).

69 G_q activation of the Trio RhoGEF leads to activation of the small GTP-binding protein Rho,
70 a major cellular switch that affects a number of cellular processes, ranging from regulation of the
71 cytoskeleton to transcription (Etienne-Manneville and Hall 2002; Jaffe and Hall 2005). In *C.*
72 *elegans* neurons, Rho has been shown to regulate synaptic transmission downstream of the G_{12} -
73 class G protein GPA-12 via at least two pathways, one dependent on the diacylglycerol kinase
74 DGK-1 and one independent of DGK-1 (McMullan *et al.* 2006; Hiley *et al.* 2006). Here we
75 investigate what targets operate downstream of Rho in the G_q signaling pathway to regulate
76 neuronal activity. Through two forward genetic screens, we identify the cation channels NCA-1
77 and NCA-2 (NALCN in mammals) as downstream targets of the G_q -Rho pathway. The NALCN
78 channel is a relative of voltage-gated cation channels that has been suggested to be a sodium
79 leak channel required for the propagation of neuronal excitation and the fidelity of synaptic
80 transmission (Lu *et al.* 2007; Jospin *et al.* 2007; Yeh *et al.* 2008). However, there is controversy
81 over the current carried by NALCN and whether it is indeed a sodium leak channel (Senatore *et*
82 *al.* 2013; Senatore and Spafford 2013; Boone *et al.* 2014). It is also unclear how NALCN is gated
83 and what pathways activate the channel. Two studies have shown that NALCN-dependent
84 currents can be activated by G protein-coupled receptors, albeit independently of G proteins (Lu *et*
85 *al.* 2009; Swayne *et al.* 2009), and another study showed that the NALCN leak current can be
86 activated by low extracellular calcium via a G protein-dependent pathway (Lu *et al.* 2010). Our
87 data presented here suggest that the worm NALCN orthologs NCA-1 and NCA-2 are activated by
88 Rho acting downstream of G_q in a linear pathway.

89

Materials and Methods

Strains

Worm strains were cultured and maintained using standard methods (Brenner, 1974). A complete list of strains and mutations used is provided in the strain list (Table S1).

Isolation of suppressors of activated G_q

We performed an ENU mutagenesis to screen for suppressors of the hyperactive locomotion of an activated G_q mutant, *egl-30(tg26)* (Ailion *et al.* 2014). From approximately 47,000 mutagenized haploid genomes, we isolated 10 mutants that had a fainter phenotype when outcrossed away from the *egl-30(tg26)* mutation. By mapping and complementation testing, we assigned these ten mutants to three genes: three *unc-79* mutants (*yak37*, *yak61*, and *yak73*), six *unc-80* mutants (*ox329*, *ox330*, *yak8*, *yak35*, *yak36*, and *yak56*) and one *nlf-1* mutant (*ox327*). Complementation tests of *ox329* and *ox330* were performed by crossing heterozygous mutant males to *unc-79(e1068)* and *unc-13(n2813) unc-80(ox301)* hermaphrodites. Complementation tests of *yak* alleles were performed by crossing heterozygous mutant males (*m/+*) to *unc-79(e1068)* and *unc-80(ox330)* mutant hermaphrodites. For all crosses, we assessed the fainting phenotype of at least five male cross-progeny by touching animals on the head and scoring whether animals fainted within five seconds. For the crosses to *unc-13 unc-80*, we also scored the fainting phenotype of at least ten Non-Unc-13 hermaphrodites similarly. Control crosses with wild-type males demonstrated that *unc-79/+* and *unc-80/+* heterozygous males and hermaphrodites are phenotypically wild-type and do not show fainting behavior, demonstrating that these mutants are fully recessive.

Isolation of suppressors of activated G_o

We first isolated suppressors of the activated G_o mutant *unc-109(n499)* by building double mutants of *unc-109(n499)* with the activated G_q allele *egl-30(tg26)*. Unlike *unc-109(n499)* homozygotes which are lethal, *egl-30(tg26) unc-109(n499)* homozygotes are viable, but paralyzed and sterile, indicating that activated G_q partially suppresses activated G_o , consistent with the model that these two G proteins act antagonistically. We built a balanced heterozygote strain *egl-30(tg26) unc-109(n499)/egl-30(tg26) unc-13(e51) gld-1(q126)* which has an “unmotivated” phenotype in which the worms move infrequently and slowly. We mutagenized these animals with ENU and screened for F1 progeny that moved better. From a screen of approximately 16,000 mutagenized haploid genomes, we isolated two apparent *unc-109* intragenic mutants, *ox303* and *ox304*. *ox303* is a strong *unc-109* loss-of-function allele, as evidenced by the fact that *egl-30(tg26) unc-109(n499 ox303)/egl-30(tg26) unc-13(e51) gld-1(q126)* mutants resembled *egl-30(tg26) unc-109(n499 ox303)* mutants themselves are hyperactive (i.e. hyperactive). Additionally, *unc-109(n499 ox303)* mutants themselves are hyperactive in an otherwise wild-type background. *ox304*, however, appears to be a partial loss-of-function mutant, because the *egl-30(tg26) unc-109(n499 ox304)/egl-30(tg26) unc-13(e51) gld-1(q126)* mutant moves better than the *egl-30(tg26) unc-109(n499)/egl-30(tg26) unc-13(e51) gld-1(q126)* parent strain, but is not hyperactive like the *egl-30(tg26)* strain. Also, *unc-109(n499 ox304)* homozygote animals on their own are viable but are almost paralyzed and show very little spontaneous movement, with a typical straight posture. However, when stimulated by transfer to a new plate, the *unc-109(n499 ox304)* mutant is surprisingly capable of coordinated movements. This strain was used for mapping and sequencing experiments that demonstrated that *unc-109* is allelic to *goa-1*, encoding the worm G_o ortholog (see below). The *unc-109(n499 ox304)* strain was also used as the starting point for a second screen to isolate extragenic suppressors of activated G_o .

Previously, a screen for suppressors of activated *goa-1* was performed using heat-shock induced expression of an activated *goa-1* transgene (Hajdu-Cronin *et al.* 1999). This screen

isolated many alleles of *dgk-1*, encoding diacylglycerol kinase, but only a single allele of *eat-16*, encoding a regulator of G protein signaling (RGS) protein that negatively regulates G_q (Hajdu-Cronin *et al.* 1999), along with mutants in three genes needed for expression of the heat-shock *goa-1* transgene (Hajdu-Cronin *et al.* 2004). Because of the strong bias of this screen for isolating alleles of *dgk-1*, we used the *goa-1(n499 ox304)* strain to perform a screen for suppressors of activated G_o that did not involve overexpression of *goa-1* or rely on expression of a heat-shocked induced *goa-1* transgene. We performed ENU mutagenesis of *goa-1(n499 ox304)* and isolated F2 animals that were not paralyzed. From a screen of approximately 24,000 mutagenized haploid genomes, we isolated 17 suppressors, 9 with a relatively stronger suppression phenotype and 8 that were weaker. Of the 9 stronger suppressors, we isolated two alleles of *eat-16* (*ox359*, *ox360*), three alleles of the BK type potassium channel *slo-1* (*ox357*, *ox358*, *ox368*), one allele of the gap junction innexin *unc-9* (*ox353*), one gain-of-function allele in the ion channel gene *nca-1* (*ox352*), and two mutants that were mapped to chromosomal regions distinct from the other mutations listed above, but not further characterized (*ox356*, *ox364*). The G_o suppressors we isolated are consistent with the established model that activation of GOA-1 activates the RGS EAT-16, which inhibits G_q EGL-30 (Hajdu-Cronin *et al.* 1999). Reduced G_q activity leads to reduced activation of the NCA cation channels, which can be reversed by an activating mutation in NCA-1. Previously, it has been shown that lack of the depolarizing NCA cation currents can be suppressed by a compensatory loss of the hyperpolarizing potassium current from SLO-1 (Kasap *et al.* 2017), or by loss of the gap junction proteins UNC-9 or UNC-7 (Sedensky and Meneely 1987; Morgan and Sedensky 1995; Bouhours *et al.* 2011). This is consistent with our isolation of *slo-1* and *unc-9* mutants as suppressors of activated G_o , since activation of G_o also leads to reduced NCA activity.

Mapping and cloning *nlf-1(ox327)*

We mapped the *ox327* mutation using single nucleotide polymorphisms (SNPs) in the Hawaiian strain CB4856 as described (Davis et al., 2005). The *ox327* mutation was mapped to an approximately 459 kb region on the left arm of the X chromosome between SNPs on cosmids F39H12 and C52B11 (SNPs F39H12[4] and pkP6101). This region included 74 predicted protein-coding genes. We injected cosmids spanning this region and found that injection of cosmid F55A4 rescued the *ox327* mutant phenotype. We performed RNAi to the genes on this cosmid in the *eri-1(mg366) lin-15(n744)* strain that has enhanced RNAi and found that RNAi of the gene F55A4.2 caused a weak fainter phenotype. We sequenced F55A4.2 in the *ox327* mutant and found a T to A transversion mutation in exon 1, leading to a premature stop codon at amino acid C59. We also rescued the *ox327* mutant with a transgene carrying only F55A4.2, confirming the gene identification. We subsequently obtained a deletion allele *tm3631* that has fainter and G_q suppression phenotypes indistinguishable from *ox327*. F55A4.2 was given the gene name *nlf-1* (Xie et al. 2013).

We obtained six independent *nlf-1* cDNAs that were predicted to be full-length: yk1105g4, yk1159a2, yk1188d11, yk1279a1, yk1521f8, and yk1709b10. Restriction digests suggested that all six were of the same size. We sequenced yk1159a2 and yk1279a1 and both gave the same *nlf-1* exon-intron structure, which differed from the gene-structure on Wormbase WS253 in several ways: *nlf-1* is 4 bp shorter at the 3' end of exon 5, and has a new 154 bp exon (now exon 6) not predicted on Wormbase. *nlf-1* consists of 8 exons and is predicted to encode a protein of 438 amino acids (Figure 3A). This is identical to the gene structure reported independently (Xie et al. 2013). Both sequenced cDNAs had 5'UTRs of 64 bp, with yk1159a2 (but not yk1279a1) being trans-spliced to the SL1 splice leader, and 3'UTRs of 424 bp (yk1279a1) or 429 bp (yk1159a2). The yk1279a1 cDNA was mutation-free and was cloned into a Gateway entry vector for use in rescue experiments. The full-length sequence of the yk1279a1 *nlf-1* cDNA was deposited in GenBank under accession # KX808524.

189

190 Mapping and cloning *unc-109(n499)*

191 *unc-109* was shown to be allelic to *goa-1*. First, we performed SNP mapping of both *unc-*
 192 *109(n499)* and its intragenic revertant *unc-109(n499 ox303)*, using the Hawaiian strain CB4856 as
 193 described (Davis *et al.* 2005). These experiments mapped *unc-109* to an approximately 1 Mb
 194 region in the middle of chromosome I between SNPs on cosmids D2092 and T24B1 (SNPs CE1-
 195 15 and T24B1[1]). A good candidate in this region was *goa-1*. We confirmed that *unc-109* was
 196 indeed *goa-1* by sequencing the three *unc-109* mutants: the gain-of-function allele *n499* carries a
 197 point mutation that leads to an R179C missense mutation, affecting a conserved arginine residue
 198 shown to be important for the GTPase activity of G proteins (Coleman *et al.* 1994); the partial loss-
 199 of-function allele *ox304* carries a point mutation leading to a W259R missense mutation; and the
 200 strong loss-of-function allele *ox303* carries a one basepair deletion that leads to a premature stop
 201 32 amino acids from the C-terminal.

202

203 Molecular biology and transgenes

204 A complete list of constructs is provided in the plasmid list (Table S2). Most of the
 205 constructs were made using the three slot multisite Gateway system (Invitrogen). For C3
 206 transferase constructs, a promoter, an FRT-mCherry-FRT-GFP cassette (pWD178), and the C.
 207 *botulinum* C3 transferase-*unc-54* 3'UTR (cloned into a Gateway entry vector from plasmid QT#99)
 208 were combined into the pDEST R4-R3 destination vector. For *nlf-1* tissue-specific rescue
 209 constructs, a promoter, the *nlf-1* coding sequence (genomic DNA or cDNA), and a C-terminal GFP
 210 tag were cloned along with the *unc-54* 3'UTR into the pDEST R4-R3 destination vector. Promoters
 211 used were *nlf-1p* (5.7 kb upstream of the ATG), *rab-3p* (all neurons), *unc-17p* (acetylcholine
 212 neurons), *unc-17Hp* (head acetylcholine neurons) (Hammarlund *et al.* 2007), *acr-2p* (acetylcholine
 213 motor neurons), *unc-17βp* (acetylcholine motor neurons) (Charlie *et al.* 2006), and *glr-1p*

(glutamate-receptor interneurons). Extrachromosomal arrays were made by standard transformation methods (Mello *et al.* 1991). Constructs of interest were injected at 10 ng/μl with marker and carrier DNAs added to make a final total concentration of at least 100 ng/μl. For most constructs, we isolated multiple independent insertions that behaved similarly. C3 transferase extrachromosomal arrays were integrated into the genome using X-ray irradiation (4000 rads). Integrated transgenes were mapped to chromosomes and outcrossed twice before further analysis.

Locomotion assays

We performed two different assays to measure locomotion. Body bend assays measured the rate of locomotion. Radial locomotion assays measured the radial distance animals moved from a point in a given unit of time, which provides a combined measurement of different aspects of the locomotion phenotype including the rate of locomotion, waveform, and frequency of reversals. Both types of assays were performed on 10 cm plates seeded with thin lawns of OP50 bacteria. These plates were prepared by seeding 1.5 ml of stationary phase OP50 bacteria to evenly cover the entire plate surface, and then growing the bacteria for two days at room temperature. Plates were stored at 4° for up to one month before being used. For body bend assays, first-day adult worms were picked to an assay plate, allowed to rest for 30 seconds, and then body bends were counted for one minute. A body bend was defined as the movement of the worm from maximum to minimum amplitude of the sine wave (Miller *et al.* 1999). To minimize variation, all animals in a body bend experiment were assayed on the same plate. For radial locomotion assays, five to eight first-day adults were picked together to the center of a plate to begin the assay (time 0). Positions of the worms were marked on the lid of the plate every ten minutes for up to forty minutes. Following the assay, the distance of each point to the center was measured. For most strains, radial distances did not increase after the first ten minutes of the

assay and all data presented here are for the ten-minute time point. Analysis of the data at later time points leads to the same conclusions. For all locomotion assays, the experimenter was blind to the genotypes of the strains being assayed.

For Rho inhibition experiments (Figure 1), expression of C3 transferase (C3T) was induced by FLP-mediated recombination. Expression of FLP was induced by heat shock for 1 hr at 34°C, plates were returned to room temperature, and animals were scored for locomotion 4 hrs after the end of the heat shock period. For heat-shock induction of activated Rho (Figure 8), worms were heat shocked for 1 hr at 34°C, returned to room temperature, and scored for locomotion 2 hrs after the end of the heat-shock period.

Fainting assays

Backward fainting times were measured by touching a worm on the head with a worm pick to stimulate movement, and measuring the time to faint with a stopwatch. Forward fainting time was measured following a touch on the tail. Fainting was defined by an abrupt stop of movement along with a characteristic straightening of the head (Figure 6A). Alternatively, we touched worms on the head or tail with a pick and counted the number of body bends until the worm fainted. If a worm moved 10 body bends without fainting, we stopped the assay.

Waveform quantification

To quantify the track waveform, first-day adult animals were placed on an OP50 plate and allowed to move forward for a few seconds. We then imaged each animal's tracks using a Nikon SMZ18 microscope with the DS-L3 camera control system. Track pictures were taken at 40X and were processed using ImageJ. Period and 2X amplitude were measured using the line tool. For each worm, five period/amplitude ratios were averaged. Five individual worms were used per experiment.

The exaggerated waveform of *egl-30(tg26)* mutants is also characterized by the head of the worm occasionally crossing over the body, leading the worm to form a figure-eight shape (Figure 2A). This phenotype was quantified by placing animals on OP50 plates and allowing them to move forward, counting the number of times the head crossed over the body in one minute.

Imaging and image analysis

Worms were mounted on 2% agarose pads and anesthetized with sodium azide. Images were obtained using a Zeiss Pascal confocal microscope. For quantitative imaging of NCA-1::GFP and NCA-2::GFP (Figure S1), Z-stack projections of the nerve ring axons on one side of the animal were collected and quantified in ImageJ as described (Jospin *et al.* 2007). Dissecting microscope photographs of first-day adult worms were taken at 50X using a Nikon SMZ18 microscope equipped with a DS-L3 camera control system.

Statistics

P values were determined using GraphPad Prism 5.0d (GraphPad Software). Normally distributed data sets with multiple comparisons were analyzed by a one-way ANOVA followed by a Bonferroni or Tukey posthoc test to examine selected comparisons or by Dunnett's test if all comparisons were to the wild type control. Non-normally distributed data sets with multiple comparisons were analyzed by a Kruskal-Wallis nonparametric ANOVA followed by Dunn's test to examine selected comparisons. Pairwise data comparisons were analyzed by a two-tailed unpaired t test for normally distributed data or by a two-tailed Mann-Whitney test for non-normally distributed data.

Reagent and data availability

288 Strains and plasmids are shown in Table S1 and Table S2 and are available from the
 289 *Caenorhabditis* Genetics Center (CGC) or upon request. The full-length sequence of the
 290 yk1279a1 *nlf-1* cDNA was deposited in GenBank under accession # KX808524. The authors state
 291 that all data necessary for confirming the conclusions presented in the article are represented fully
 292 within the article and Supplemental Material.
 293

Results

Inhibition of Rho suppresses activated G_q

Two pieces of data suggested that G_q may regulate locomotion in *C. elegans* through activation of the small G protein Rho. First, both the hyperactive locomotion and tightly wound body posture of the activated G_q mutant *egl-30(tg26)* are suppressed by loss-of-function mutations in the *unc-73* RhoGEF Trio, an activator of Rho (Williams *et al.* 2007). Second, expression of activated Rho as a transgene causes worms to adopt a posture characterized by a tightly coiled, high-amplitude waveform (McMullan *et al.* 2006), reminiscent of the waveform of activated G_q worms (Bastiani *et al.* 2003; Ailion *et al.* 2014). To determine directly whether G_q signals through Rho, we tested whether Rho inhibition suppresses an activated G_q mutant.

In *C. elegans*, there is a single gene encoding Rho (*rho-1*). Loss of *rho-1* causes numerous pleiotropic developmental phenotypes and embryonic lethality (Jantsch-Plunger *et al.* 2000), making it difficult to study Rho function using classical loss-of-function approaches. As an alternative method of inactivating Rho, we employed the *Clostridium botulinum* C3 transferase (C3T) which ADP-ribosylates Rho and has been widely used as a Rho inhibitor (Aktories *et al.* 2004). C3T has strong substrate specificity for Rho and has only weak activity towards other Rho family members like Rac and Cdc42 (Just *et al.* 1992). Though effects of C3T on targets other than Rho cannot be absolutely excluded, a study in *C. elegans* found that C3T, *rho-1* RNAi, and expression of a dominant-negative form of Rho all caused similar defects in P cell migration (Spencer *et al.* 2001). To bypass the developmental roles and study Rho function in the adult nervous system, we expressed the C3T only in adult neurons by using the FLP recombinase/FRT system (Davis *et al.* 2008). In this system, temporal control of C3T is achieved through induction of FLP via heat-shock. FLP in turn promotes recombination between FRT sites to lead to expression of C3 transferase in specific neurons (Figure 1A). We expressed C3T in the following

classes of neurons: all neurons (*rab-3p*), acetylcholine neurons (*unc-17p*), head acetylcholine neurons (*unc-17Hp*), and acetylcholine motor neurons (*unc-17βp*). mCherry fluorescence confirmed expression in the expected neurons and GFP expression was used to monitor induction of C3T following FLP-mediated recombination.

Inhibition of *rho-1* in adult neurons caused a decreased locomotion rate (Figure 1B). This effect was greatest when Rho was inhibited in all neurons, but Rho inhibition in acetylcholine subclasses of neurons also led to slower locomotion. Thus, Rho acts in multiple classes of neurons to promote locomotion in adult worms. In the absence of heat-shock, all strains showed normal wild-type rates of locomotion and did not express any detectable GFP, indicating that these transgenes do not provide leaky expression of C3T in the absence of heat-shock. This confirms that Rho acts post-developmentally in mature neurons to regulate locomotion behavior (McMullan *et al.* 2006).

To determine whether Rho acts downstream of G_q signaling, we crossed the C3 transgenes into the background of the activated G_q mutant *egl-30(tg26)*. Inhibition of *rho-1* in all adult neurons strongly suppressed the high-amplitude waveform, body posture, and hyperactive locomotion of the activated G_q mutant (Figure 1, C-F). Inhibition of *rho-1* in acetylcholine neurons suppressed the hyperactivity of activated G_q (Figure 1C), but only weakly suppressed the high-amplitude waveform (Figure 1, D-F). Thus, *rho-1* exhibits genetic interactions consistent with a role in the G_q signaling pathway in both acetylcholine neurons and additional neurons.

Mutations in NCA channel subunits suppress activated G_q

What acts downstream of Rho in the G_q signal transduction pathway? We screened for suppressors of activated G_q and found mutants in three categories: (1) the canonical G_q pathway (such as the PLC *egl-8*); (2) the RhoGEF *unc-73* (Williams *et al.* 2007), and (3) genes that affect dense-core vesicle function (*e.g.* *unc-31*, *rab-2*, *rund-1*) (Ailion *et al.* 2014; Topalidou *et al.* 2016).

Mutations in *unc-73* strongly suppress the high-amplitude waveform of the activated G_q mutant (Figure 2, A and C), but mutations in the canonical G_q pathway or in genes that affect dense-core vesicle function only weakly suppress the high-amplitude waveform of the activated G_q mutant (Figure 2). Thus, strong suppression of the high-amplitude waveform of activated G_q may be a specific characteristic of mutations in the Rho pathway, and we hypothesized that downstream targets of Rho in this pathway would also suppress the high-amplitude waveform.

To identify possible downstream targets of Rho in the G_q pathway, we examined other mutants isolated from our screen for suppression of the high-amplitude waveform of activated G_q (Figure 2). When crossed away from the activating G_q mutation, several of these mutants had a “fainter” phenotype. Fainter mutants respond to a touch stimulus by moving away, but abruptly stop, that is “faint”, after only a few body bends. The fainter phenotype has been observed only in mutants that reduce the function of the NCA-1 and NCA-2 ion channels (Humphrey *et al.* 2007; Jospin *et al.* 2007; Yeh *et al.* 2008). We found that all our G_q suppressors that strongly suppressed the high-amplitude waveform and had a fainter phenotype were mutants in either *unc-79* or *unc-80*, two genes required for function of the NCA channels (Humphrey *et al.* 2007; Jospin *et al.* 2007; Yeh *et al.* 2008). We also isolated a single mutant in the gene *nlf-1* that also gave fainters after outcrossing away from the activated G_q mutation, but did not strongly suppress the high-amplitude waveform of the activated G_q mutant (Figure 2). *unc-79* and *unc-80* mutants have a strong fainter phenotype equivalent to that of a double mutant in *nca-1* and *nca-2*, two genes that encode pore-forming subunits of the NCA channels in *C. elegans* (Humphrey *et al.* 2007; Jospin *et al.* 2007; Yeh *et al.* 2008). Like *unc-79* or *unc-80*, an *nca-1 nca-2* double mutant suppressed the activated G_q mutant. Additionally, *nca-1* on its own partially suppressed activated G_q, but *nca-2* did not (Figure 2). This suggests that although *nca-1* and *nca-2* are only redundantly required for normal worm locomotion, channels containing the NCA-1 pore-forming subunit have a larger role in transducing G_q signals than NCA-2 channels.

369

370 **Cloning and characterization of *nlf-1(ox327)***

371 In addition to the previously known NCA channel subunits *unc-79* and *unc-80*, we also
372 isolated the *ox327* mutant in a gene that had not been previously characterized at the time of our
373 study. We cloned *ox327* by single nucleotide polymorphism (SNP) mapping, RNAi and transgenic
374 rescue experiments (see Materials and Methods), showing that it carries an early stop mutation in
375 the gene *nlf-1*. We sequenced two *nlf-1* cDNAs and found that its exon-intron structure differed
376 from the gene structure predicted on Wormbase (Figure 3A, see Materials and Methods for
377 details). *nlf-1* was independently cloned by others (Xie *et al.* 2013).

378 *nlf-1* encodes an endoplasmic reticulum-localized protein probably involved in proper
379 assembly of the NCA channel, since *nlf-1* mutants had reduced expression levels of GFP-tagged
380 NCA-1 and NCA-2 (Xie *et al.* 2013). We also found that *nlf-1* is required for normal axonal levels
381 of both GFP-tagged NCA-1 and NCA-2 in the nerve ring (Figure S1). Additionally, an *nlf-1*
382 mutation suppressed both the coiled posture and slow locomotion of an activated *nca-1* mutant
383 (Figure 3, B-F), demonstrating that *nlf-1* is important for NCA-1 function.

384 *nlf-1* mutants have a weaker fainter phenotype than mutants of *unc-79* or *unc-80*, or the
385 *nca-1 nca-2* double mutant (Figure 4, A and B). The *nlf-1* fainting phenotype differs in two ways
386 from those of the stronger fainting mutants. First, *nlf-1* mutants take a longer time to faint following
387 stimulation (Figure 4, A and B). Second, while the strong fainting mutants show a similarly strong
388 fainting phenotype in either the forward or backward direction, *nlf-1* mutants faint reliably in the
389 backward direction but take much longer and have more variable fainting in the forward direction
390 (Figure 4, A and B), suggesting that *nlf-1* mutations cause a partial loss of function of the NCA
391 channels. To determine how *nlf-1* interacts with NCA mutants, we built *nlf-1(ox327)* double
392 mutants with *unc-79*, *unc-80*, *nca-1*, and *nca-2*. The *nlf-1* mutation did not enhance the *unc-79* or
393 *unc-80* fainter phenotype, suggesting that these mutants act in the same pathway to control

fainting (Figure 4, C and D). However, *nca-1* strongly enhanced the *nlf-1* fainter phenotype, but *nca-2* did not significantly enhance *nlf-1* (Figure 4, A and B). Neither *nca-1* nor *nca-2* single mutants have a fainter phenotype on their own (Humphrey *et al.* 2007), but the fact that an *nca-1 nlf-1* double mutant has a strong fainter phenotype suggests that either *nca-1* contributes more than *nca-2* for normal locomotion or that *nlf-1* specifically perturbs function of *nca-2*. Our data presented below are more consistent with the possibility that *nca-1* contributes more than *nca-2* to wild-type locomotion behavior.

We determined the cellular expression pattern of *nlf-1* by fusing its promoter to GFP. *nlf-1p::GFP* was expressed in most or all neurons, but was not detected in other tissues (Figure 5A). This agrees with the expression pattern reported elsewhere (Xie *et al.* 2013). To determine the neuronal focus of the fainter phenotype, we performed rescue experiments in which we determined whether an *nlf-1* mutant could be rescued by expression of a wild-type *nlf-1* cDNA under the control of neuron-specific promoters. Expression of *nlf-1(+)* in all neurons (using the *rab-3* promoter) or acetylcholine neurons (using the *unc-17* promoter) fully rescued the *nlf-1* mutant fainter phenotype (Figure 5B). Expression in acetylcholine motor neurons (using the *acr-2* or *unc-17 β* promoters) did not rescue the fainter phenotype, but expression driven by a head-specific derivative of the *unc-17* promoter (*unc-17Hp*) fully rescued the fainter phenotype, indicating that the action of *nlf-1* in head acetylcholine neurons is sufficient to prevent fainting (Figure 5B).

Previously, it was reported that expression of *nlf-1* in premotor interneurons is sufficient to rescue the *nlf-1* mutant fainter phenotype (Xie *et al.* 2013). However, we found that expression of *nlf-1* in premotor interneurons using the *glr-1* promoter (*glr-1p*) had only a weak effect on the *nlf-1* mutant fainter phenotype and did not fully restore wild-type locomotion (Figure 5C). Fainting behavior was difficult to score in the *glr-1* promoter-rescued *nlf-1* mutant animals because they had sluggish movement and stopped frequently, though generally not with the suddenness and characteristic posture typical of fainters. Though we could blindly score the rescue of fainting in

these animals by eye, we saw only weak rescue of the *nlf-1* mutant by *glr-1* promoter expression in our quantitative fainting assays and the effect was not statistically significant (Figure 5C). When we instead measured fainting as the percentage of animals that fainted within ten body bends, we did see a marginally significant rescue by *glr-1* promoter expression (backward fainting: *nlf-1* = 92%, *nlf-1; glr-1p::nlf-1(+)* = 68%, $P=0.0738$, Fisher's exact test; forward fainting: *nlf-1* = 80%, *nlf-1; glr-1p::nlf-1(+)* = 48%, $P=0.0378$, Fisher's exact test). We may be underestimating the rescue of the fainting phenotype by *glr-1* promoter expression due to the difficulty distinguishing the frequent pausing from true fainting. Nevertheless, rescue of the *nlf-1* mutant is clearly stronger by expression in head acetylcholine neurons using the *unc-17H* promoter (Figure 5B). Though our data seem to contradict the previous study reporting that *nlf-1* acts in premotor interneurons (Xie *et al.* 2013), there are several possible explanations. First, like our data, the data in the previous study in fact showed only partial rescue of fainting behavior by expression in premotor interneurons (Xie *et al.* 2013). Second, the premotor interneuron promoter combination used in the previous study (*nmr-1p + sra-11p*) leads to expression in several other head interneurons that may contribute to the phenotype. Third, it is possible that rescue is sensitive to expression level and that different levels of expression were achieved in the two studies, leading to different levels of rescue. We conclude that NLF-1 acts in head acetylcholine neurons, including the premotor interneurons, to promote sustained locomotion in the worm. Consistent with this, the premotor command interneurons have recently been shown to use acetylcholine as a neurotransmitter (Pereira *et al.* 2015).

Mutations in NCA channel subunits suppress activated Rho

To determine whether NCA mutants act downstream of Rho, we took advantage of an activated Rho mutant (G14V) expressed specifically in the acetylcholine neurons (McMullan *et al.* 2006). Like an activated G_q mutant, this activated Rho mutant has an exaggerated waveform. We

built double mutants of the activated Rho mutant with mutations in *unc-79*, *unc-80*, *nlf-1* and mutations in the NCA channel genes *nca-1* and *nca-2*. The *nca-1* and *nca-2* genes are redundant for the fainter phenotype because neither mutant has a fainter phenotype individually, but the double mutant has a fainter phenotype indistinguishable from *unc-79* and *unc-80* mutants (Humphrey *et al.* 2007; Jospin *et al.* 2007; Yeh *et al.* 2008). We found that the high-amplitude waveform caused by activated Rho was strongly suppressed in *unc-80* mutants, as well as in *nca-1 nca-2* double mutants (Figure 6). In both cases, the resulting double or triple mutants had a fainter phenotype like the *unc-80* or *nca-1 nca-2* mutants on their own. By contrast, the high-amplitude waveform of activated Rho was incompletely suppressed by a mutation in *nlf-1*, consistent with the *nlf-1* mutation causing only a partial loss of NCA channel function (Figure 6). Reciprocally, activated Rho suppressed the weak fainter phenotype of an *nlf-1* mutant, again because Rho can act on NCA even in the absence of *nlf-1*. Additionally, a mutation in *nca-1* also partially suppressed the high-amplitude waveform of activated Rho, but a mutation in *nca-2* did not suppress the high-amplitude waveform (Figure 6). Thus, channels containing the NCA-1 pore-forming subunit have a larger role than NCA-2 channels in transducing Rho signals, similar to the interaction of NCA-1 and G_q signaling.

Because an activated Rho mutant has slow locomotion (Figure 7A) and *unc-79*, *unc-80*, and *nca-1 nca-2* double mutants also have slow locomotion, it is difficult to determine whether these NCA channel mutants suppress the locomotion phenotype of activated Rho in addition to its waveform. We performed radial locomotion assays that provide a combined measurement of several aspects of the locomotion phenotype, including the rate of movement, frequency of reversals, and amplitude of the waveform (see Materials and Methods). By these assays, mutations in *unc-80* or *nca-1 nca-2* lead to only small increases in the radial distance traveled by an activated Rho mutant and an *nca-2* mutant had no effect (Figure 7B). However, a mutation in *nlf-1* much more strongly increased the radial distance traveled by an activated Rho mutant.

Because the *nlf-1* mutant is not as slow on its own, we could also directly assay its effect on the rate of locomotion of an activated Rho mutant by counting the number of body bends per minute. An *nlf-1* mutation strongly increased the rate of locomotion of an activated Rho mutant (Figure 7A). In fact, the *nlf-1* double mutant with activated Rho had a faster rate of locomotion than either activated Rho or *nlf-1* on its own, similar to the effect of *nlf-1* on the locomotion of an activated *nca-1* mutant (Figure 3E). Additionally, a mutation in *nca-1* strongly increased the locomotion rate of the activated Rho mutant, but a mutation in *nca-2* had no effect (Figure 7A), further supporting the idea that NCA channels consisting of the NCA-1 subunit act downstream of G_q and Rho in this pathway.

Rho regulates worm locomotion independently of effects on development, as demonstrated by the fact that heat-shock induction of an activated Rho transgene in adults leads to a high-amplitude waveform similar to that seen in worms that express activated Rho in acetylcholine neurons (McMullan *et al.* 2006). Consistent with the idea that NCA-1 acts downstream of Rho, mutations in the fainter genes *unc-80* and *nlf-1* suppress the high-amplitude waveform phenotype of heat-shock induced activated Rho (Figure 8, A-C). Additionally, *nlf-1* also suppresses the locomotion defect of heat-shock induced activated Rho (Figure 8D). Thus, Rho regulates worm locomotion via the NCA channels by acting in a non-developmental pathway that operates in adult neurons.

A dominant NCA-1 mutation suppresses activated G_o

In *C. elegans*, the G_q pathway is opposed by signaling through the inhibitory G_o protein GOA-1 (Hajdu-Cronin *et al.* 1999; Miller *et al.* 1999). Thus, loss-of-function mutants in *goa-1* are hyperactive and have a high-amplitude waveform, similar to the gain-of-function G_q mutant *egl-30(tg26)*. We found that the uncloned dominant mutant *unc-109(n499)* which is paralyzed and resembles loss-of-function mutants in *egl-30* (Park and Horvitz 1986) carries an activating

mutation in *goa-1* (see Materials and Methods). The *goa-1(n499)* mutant is paralyzed as a heterozygote, and is lethal as a homozygote (Park and Horvitz 1986). We performed a screen for suppressors of *goa-1(n499)* and isolated a partial intragenic suppressor, *goa-1(n499 ox304)* (Materials and Methods). *goa-1(n499 ox304)* homozygote animals are viable but are almost paralyzed and show very little spontaneous movement, with a straight posture and low-amplitude waveform (Figure 9, C and D). However, when stimulated, the *goa-1(n499 ox304)* mutant is capable of slow coordinated movements (Figure 9, A and B).

We mutagenized the *goa-1(n499 ox304)* strain and screened for animals that were not paralyzed or did not have a straight posture. Among the suppressors, we isolated a mutant (*ox352*) that was found to be a dominant gain-of-function mutation in the *nca-1* gene (Bend *et al.* 2016). The *nca-1(ox352)* mutant has a coiled posture and high-amplitude waveform reminiscent of the activated G_q and activated Rho mutants (Figure 3B). Furthermore, *nca-1(ox352)* suppresses the straight waveform of the activated G_o mutant *goa-1(n499 ox304)* (Figure 9, C and D). Thus, activation of NCA-1 suppresses activated G_o whereas loss of NCA-1 suppresses activated G_q , both consistent with the model that G_o inhibits G_q and that NCA-1 is a downstream effector of the G_q pathway.

Discussion

In this study, we identify the NCA-1 and NCA-2 ion channels as downstream effectors of the heterotrimeric G proteins G_o and G_q . Previously, it has been demonstrated that activation of $G_o\alpha$ GOA-1 activates the RGS protein EAT-16, which in turn inhibits $G_q\alpha$ (Hajdu-Cronin *et al.* 1999; Miller *et al.* 1999). Loss of *goa-1* leads to hyperactive worms (Mendel *et al.* 1995; Ségalat *et al.* 1995). Here we identified an activated mutation in *goa-1* that causes animals to be paralyzed, closely resembling null mutations in the $G_q\alpha$ gene *egl-30* (Brundage *et al.* 1996). Suppressors of activated G_o include loss-of-function mutations in the RGS EAT-16, and gain-of-function mutations in the NCA-1 channel, suggesting that activated G_o inactivates G_q , and could thereby indirectly inactivate the NCA-1 cation channel.

Further genetic epistasis data indicate that G_q activates the RhoGEF Trio and the small GTPase Rho. Rho then acts via an unknown mechanism to activate the NCA-1 and NCA-2 ion channels, which are required for normal neuronal activity and synaptic transmission in *C. elegans* (Jospin *et al.* 2007; Yeh *et al.* 2008; Xie *et al.* 2013; Gao *et al.* 2015). Thus, this work identifies a new genetic pathway from G_q to an ion channel that regulates neuronal excitability and synaptic release: $G_q \rightarrow \text{RhoGEF} \rightarrow \text{Rho} \rightarrow \text{NCA channels}$ (Figure 10). The NCA channels have not been previously identified as effectors of the G_q pathway, so this pathway may give insight into how the NCA channels are activated or regulated.

Mutations that eliminate the NCA channels, such as *unc-80* or the *nca-1 nca-2* double mutant, suppress the locomotion and body posture phenotypes of an activated Rho mutant (Figures 6-8), suggesting that NCA channels act downstream of Rho in a linear pathway. Additionally, channels composed of the pore-forming subunit NCA-1 may be the main target of G_q -Rho signaling. First, loss-of-function mutations in *nca-1* alone, but not *nca-2*, partially suppress activated G_q and activated Rho mutants. Second, activating gain-of-function mutants of *nca-1* have phenotypes reminiscent of activated G_q and activated Rho mutants, but no activated mutants

in *nca-2* have been isolated. Third, loss-of-function mutations in *nca-1*, but not *nca-2*, enhance the weaker fainting phenotype of an *nlf-1* mutant which does not fully eliminate function of the NCA channels. Together these data suggest that although either NCA-1 or NCA-2 activity is sufficient for wild-type locomotion, NCA-1 is likely to be the main target of G protein regulation.

We characterized three locomotory behaviors in this manuscript: locomotion rate, waveform, and fainting. The G_q -Rho-NCA pathway regulates all three behaviors, but our genetic epistasis and cell-specific rescue experiments suggest that these behaviors are differentially regulated and involve at least partially distinct sets of neurons. First, the hyperactive locomotion and high-amplitude waveform phenotypes of the activated G_q mutant are genetically separable, since they are differentially suppressed by mutations in the PLC β pathway and the Rho-NCA pathway. Mutations in the Rho-NCA pathway suppress both the locomotion rate and high-amplitude waveform of activated G_q whereas mutations in the PLC β pathway suppress the locomotion rate but only very weakly suppress the high-amplitude waveform of activated G_q . Thus, G_q acts through both the PLC β pathway and the Rho-NCA pathway to regulate locomotion rate, but primarily through the Rho-NCA pathway to regulate the waveform of the animal. Second, we found that NLF-1 activity in head acetylcholine neurons is sufficient to fully rescue the fainting phenotype of an *nlf-1* mutant. However, inhibition of Rho in the head acetylcholine neurons did not suppress the high-amplitude waveform of the activated G_q mutant, but inhibition of Rho in all neurons did suppress. This suggests that Rho does not act solely in head acetylcholine neurons to regulate the waveform. Thus, the G_q -Rho-NCA pathway acts in at least two different classes of neurons to regulate fainting and waveform.

It is not clear whether Rho activation of the NCA channels is direct or indirect. G_q directly interacts with and activates the RhoGEF and Rho, as shown by the crystal structure of a complex between $G_q\alpha$, RhoGEF, and Rho (Lutz *et al.* 2007). Rho is known to have many possible effectors and actions in cells (Etienne-Manneville and Hall 2002; Jaffe and Hall 2005). In *C. elegans*

neurons, Rho has been previously shown to regulate synaptic transmission via at least two pathways, one involving a direct interaction of Rho with the DAG kinase DGK-1 and one that is DGK-1 independent (McMullan *et al.* 2006). A candidate for the link between Rho and NCA is the type I phosphatidylinositol 4-phosphate 5-kinase (PIP5K) that synthesizes the lipid phosphatidylinositol 4,5,-bisphosphate (PIP2). PIP5K is an intriguing candidate for several reasons. First, activation of G_q in mammalian cells has been shown to stimulate the membrane localization and activity of PIP5K via a mechanism that depends on Rho (Chatah and Abrams 2001; Weernink *et al.* 2004). Second, in *C. elegans*, mutations eliminating either the NCA channels (*nca-1 nca-2* double mutant) or their accessory subunits (*unc-79* or *unc-80*) suppress mutants in the PIP2 phosphatase synaptojanin (*unc-26*) and also suppress phenotypes caused by overexpression of the PIP5K gene *ppk-1* (Jospin *et al.* 2007). Loss of a PIP2 phosphatase or overexpression of a PIP5K are both predicted to increase levels of PIP2. Because the loss of NCA channels suppresses the effects of too much PIP2, it is possible that excessive PIP2 leads to overactivation of NCA channels and that PIP2 might be part of the normal activation mechanism. There are numerous examples of ion channels that are regulated or gated by phosphoinositide lipids such as PIP2 (Balla 2013), though PIP2 has not been shown to directly regulate NCA/NALCN.

The NCA/NALCN ion channel was discovered originally by bioinformatic sequence analyses (Lee *et al.* 1999; Littleton and Ganetzky 2000). It is conserved among all metazoan animals and is evolutionarily-related to the family of voltage-gated sodium and calcium channels (Liebeskind *et al.* 2012), forming a new branch in this super-family. Although the cellular role of the NCA/NALCN channel and how it is gated are not well understood, NALCN and its orthologs are expressed broadly in the nervous system in a number of organisms (Lee *et al.* 1999; Lear *et al.* 2005; Humphrey *et al.* 2007; Lu *et al.* 2007; Jospin *et al.* 2007; Yeh *et al.* 2008; Lu and Feng 2011; Lutas *et al.* 2016). Moreover, mutations in this channel or its auxiliary subunits lead to

defects in rhythmic behaviors in multiple organisms (Lear *et al.* 2005, 2013; Lu *et al.* 2007; Jospin *et al.* 2007; Yeh *et al.* 2008; Pierce-Shimomura *et al.* 2008; Xie *et al.* 2013; Funato *et al.* 2016). Thus, NCA/NALCN is likely to play an important role in controlling membrane excitability. Additionally, NALCN currents have been reported to be activated by two different G protein-coupled receptors (GPCRs), the muscarinic acetylcholine receptor and the substance P receptor, albeit in a G protein-independent fashion (Lu *et al.* 2009; Swayne *et al.* 2009), and by low extracellular calcium via a G protein-dependent pathway (Lu *et al.* 2010). The latter study further showed that expression of an activated G_q mutant inhibited the NALCN sodium leak current, suggesting that high extracellular calcium tonically inhibits NALCN via a G_q-dependent pathway and that low extracellular calcium activates NALCN by relieving this inhibition (Lu *et al.* 2010). By contrast, we find that G_q activates the NCA channels in *C. elegans*, and we show that the NCA channels are physiologically relevant targets of a G_q signaling pathway that acts through Rho.

In the last few years, both recessive and dominant human diseases characterized by a range of neurological symptoms including hypotonia, intellectual disability, and seizures have been shown to be caused by mutations in either *NALCN* or *UNC80* (Köroğlu *et al.* 2013; Al-Sayed *et al.* 2013; Chong *et al.* 2015; Aoyagi *et al.* 2015; Shamseldin *et al.* 2016; Stray-Pedersen *et al.* 2016; Gal *et al.* 2016; Fukai *et al.* 2016; Karakaya *et al.* 2016; Perez *et al.* 2016; Bend *et al.* 2016; Lozic *et al.* 2016; Valkanas *et al.* 2016; Wang *et al.* 2016; Vivero *et al.* 2017). Notably, dominant disease-causing mutations in the NALCN channel were modeled in worms and resemble either dominant activated or loss-of-function NCA mutants such as the ones we use in this study (Aoyagi *et al.* 2015; Bend *et al.* 2016). Human mutations in other components of the pathway we have described may cause similar clinical phenotypes.

Acknowledgments

610 We thank Shohei Mitani for the *nlf-1(tm3631)* mutant; Steve Nurrish for worm strains and
611 plasmids carrying activated Rho or C3 transferase; Ken Miller for a plasmid with the *unc-17β*
612 promoter; Wayne Davis for FLP/FRT plasmids; Yuji Kohara for cDNA clones; the Sanger Center
613 for cosmids; Brooke Jarvie, Jill Hoyt, and Michelle Giarmarco for the isolation of *unc-79* and *unc-*
614 *80* mutations in the G_q suppressor screen; and Dana Miller for the use of her microscope and
615 camera to take worm photographs. Some strains were provided by the CGC, which is funded by
616 NIH Office of Research Infrastructure Programs (P40 OD010440). M.A. is an Ellison Medical
617 Foundation New Scholar. E.M.J. is an Investigator of the Howard Hughes Medical Institute. This
618 work was supported by NIH grants R00 MH082109 to M.A and R01 NS034307 to E.M.J.
619

Figure Legends

Figure 1 Inhibition of Rho in neurons suppresses an activated G_q mutant. (A) Schematic of the FLP/FRT system we used for temporal and spatial expression of the Rho inhibitor C3 transferase (C3T). The transgene in the “off” configuration expresses the mCherry reporter under the control of the promoter sequence but terminates transcription in the *let-858* 3’UTR upstream of GFP-C3T. Expression of the FLP recombinase is induced by heat shock and leads to recombination between the FRT sites and deletion of the intervening *mCherry::let-858* 3’UTR fragment. This leads to transcription of GFP-C3T in the cells driven by the adjacent promoter. We used the pan-neuronal promoter *rab-3p*, acetylcholine neuron promoter *unc-17p*, and head acetylcholine neuron promoter *unc-17Hp*. (B) Inhibition of Rho in adult neurons causes a locomotion defect. Inhibition of Rho by C3 transferase (C3T) in all adult neurons (*rab-3p*, *oxIs412* transgene), acetylcholine neurons (*unc-17p*, *oxIs414* transgene) or head acetylcholine neurons (*unc-17Hp*, *oxIs434* transgene) reduces the locomotion rate of wild type animals. ***, $P < 0.001$, Dunnett’s test. Error bars = SEM; $n = 19-20$. (C) Inhibition of Rho in all adult neurons (*rab-3p*, *oxIs412* transgene) or acetylcholine neurons (*unc-17p*, *oxIs414* transgene) led to a significant reduction in the rate of locomotion of the activated G_q mutant *egl-30(tg26)* (here written G_q^*). Inhibition of Rho in head acetylcholine neurons (*unc-17Hp*, *oxIs434* transgene) led to a small decrease in G_q^* locomotion that was not statistically significant. ***, $P < 0.001$; ns, not significant, $P > 0.05$, Dunnett’s test. Error bars = SEM; $n = 10-20$. (D) Photos of first-day adult worms. The coiled body posture of the activated G_q mutant *egl-30(tg26)* (G_q^*) is suppressed by Rho inhibition in all neurons (*rab-3p::C3T*). (E) Photos of worm tracks. (F) Quantification of the track waveform. The high-amplitude waveform of the activated G_q mutant *egl-30(tg26)* (G_q^*) is suppressed by Rho inhibition in all adult neurons (*rab-3p::C3T*) and partially suppressed by Rho inhibition in acetylcholine neurons (*unc-17p::C3T*). Rho inhibition in head acetylcholine (*unc-17Hp::C3T*) neurons did not suppress the

645 waveform of Gq*. ***, P<0.001; ns, not significant, P>0.05, Bonferroni test. All comparisons are to
646 Gq*. Error bars = SEM; n = 5.

647

648 **Figure 2** Mutations affecting the NCA-1 and NCA-2 channels suppress the high-amplitude
649 waveform of the activated G_q mutant *egl-30(tg26)* (Gq*). The *unc-73(ox317)*, *unc-79(yak37)* and
650 *unc-80(ox330)* mutations suppress the high-amplitude waveform of Gq*. The *nca-1(gk9)* and *nlf-*
651 *1(ox327)* mutations partially suppress the high-amplitude waveform of Gq* as measured by the
652 crossover assay. Mutations in the canonical G_q pathway such as *egl-8(ox333)* partially suppress
653 and genes required for dense-core vesicle biogenesis such as *rund-1(tm3622)* do not significantly
654 suppress the high-amplitude waveform of Gq*. The *nca-2(gk5)* mutation does not suppress Gq*.
655 (A) Photos of first-day adults. (B) Photos of worm tracks. The photo of wild type tracks is the same
656 as the one shown in Figure 3C. (C) Quantification of the track waveform. The wild-type waveform
657 data are the same data shown in Figures 3D, 6C, and 9D. (D) Quantification of the worm's head
658 crossing its body ("crossovers"). ***, P<0.001; **, P<0.01; *, P<0.05; ns, not significant, P>0.05,
659 Bonferroni test. All comparisons are to Gq*. Error bars = SEM; n = 5 (panel C); n = 6 (panel D).

660

661 **Figure 3** The *nlf-1(ox327)* mutation suppresses the coiled posture, high-amplitude waveform, and
662 locomotion defect of the activated NCA-1 mutant *nca-1(ox352)* (Nca*). (A) Gene structure of *nlf-1*.
663 Black boxes show coding segments. White boxes show 5' and 3' untranslated regions (UTRs).
664 The *ox327* mutation leads to a premature stop codon at C59. The *tm3631* deletion removes most
665 of the 5'UTR and first exon. (B) Photos of first-day adult worms. (C) Photos of worm tracks. The
666 photo of wild type tracks is the same as the one shown in Figure 2B. (D) Quantification of track
667 waveform. The high-amplitude waveform of Nca* is suppressed by *nlf-1*. The wild-type data are
668 the same data shown in Figures 2C, 6C, and 9D. (E) Body bend assay. The wild-type data shown
669 in the left graph are the same as shown in Figure 7A, right graph. (F) Radial locomotion assay.

670 Statistics in D: ***, $P < 0.001$, two-tailed unpaired t test. Comparisons are to Nca*. Error bars =
671 SEM, $n = 5$. Statistics in E and F: ***, $P < 0.001$, two-tailed Mann-Whitney test. Error bars = SEM, n
672 = 4-10 (panel E), $n = 8-26$ (panel F).

673

674 **Figure 4** *nlf-1* mutants are weak fainters. The *nlf-1(ox327)* mutant is a weaker fainter in the
675 forward direction (A) than the backward direction (B), but *nlf-1(ox327)* has a weaker fainter
676 phenotype than either *unc-80(ox330)* or the *nca-2(gk5); nca-1(gk9)* double mutant. Additionally,
677 *nlf-1* mutants are enhanced by a mutation in *nca-1*, but not *nca-2*. Wild-type, *nca-1(gk9)*, and *nca-*
678 *2(gk5)* mutant animals are not shown in the figure because they do not faint (0/10 animals fainted
679 in a one minute period). Also, *nlf-1(ox327)* mutants do not enhance the strong forward (C) or
680 backward (D) fainting phenotypes of *unc-79(e1068)* and *unc-80(ox330)* mutants. ***, $P < 0.001$; ns,
681 not significant, $P > 0.05$, Dunn's test. Error bars = SEM; $n = 10-20$.

682

683 **Figure 5** *nlf-1* acts in head acetylcholine neurons to control locomotion. (A) *nlf-1* is expressed
684 widely in the nervous system. A fusion of the *nlf-1* promoter to GFP (transgene *oxEx1144*) is
685 expressed throughout the nervous system, including head and tail neurons, and motor neurons in
686 the ventral nerve cord. No expression is seen in non-neuronal tissues. An L1 stage larval animal is
687 shown with its head to the left. (B,C) The *nlf-1* cDNA was expressed in an *nlf-1(ox327)* mutant
688 background using the following promoters: *rab-3* (all neurons, *oxEx1146* transgene), *unc-*
689 *17* (acetylcholine neurons, *oxEx1149* transgene), *unc-17H* (a derivative of the *unc-17* promoter
690 that lacks the enhancer for ventral cord expression and thus expresses in head acetylcholine
691 neurons and occasionally a few tail neurons, *oxEx1155* transgene), *unc-17 β* (a derivative of
692 the *unc-17* promoter that expresses only in ventral cord acetylcholine neurons, *oxEx1323*
693 transgene), *acr-2* (ventral cord acetylcholine motor neurons, *oxEx1151* transgene), and *glr-1*
694 (interneurons including premotor command interneurons, *oxEx1152* transgene). (B) Expression

driven by the *rab-3*, *unc-17*, and *unc-17H* promoters rescued the fainting phenotype of an *nlf-1* mutant in the backward direction. ***, $P < 0.001$, Dunn's test. Error bars = SEM; $n = 15$. (C) Expression driven by the *glr-1* promoter partially rescued the fainting phenotype of an *nlf-1* mutant in either the backward or forward direction, though the effect was not statistically significant (ns, $P > 0.05$, two-tailed Mann-Whitney tests. Error bars = SEM; $n = 25$). However, assays of this strain were complicated by slow movement and frequent pauses that were hard to distinguish from true fainting behavior (see text for details).

Figure 6 Mutations in NCA channel subunits suppress the high-amplitude waveform of animals expressing activated Rho. Animals expressing an activated Rho mutant (G14V) in acetylcholine neurons (*nzls29* transgene, written as Rho*) have a high-amplitude waveform. Mutations that eliminate NCA-1 and NCA-2 channel function (*unc-80(ox330)* or *nca-2(gk5)*; *nca-1(gk9)*) strongly suppress the high-amplitude waveform of activated Rho and convert the activated Rho mutants to fainters. Mutations in *nlf-1(ox327)* and *nca-1(gk9)* strongly but incompletely suppress the high-amplitude waveform of activated Rho and these double mutants do not faint. Mutations in *nca-2(gk5)* do not suppress the high-amplitude waveform of activated Rho. Mutants in *unc-80*, *nlf-1*, and the *nca-2 nca-1* double mutant have the typical fainter posture characterized by a straightened anterior part of the body. (A) Photos of first-day adult worms. (B) Photos of worm tracks. (C) Quantification of track waveform. The wild-type data are the same data shown in Figures 2C, 3D, and 9D. ***, $P < 0.001$; **, $P < 0.01$; ns, not significant, $P > 0.05$, Bonferroni test. All comparisons are to Rho*. Error bars = SEM; $n = 5$.

Figure 7 Mutations in *nlf-1* and *nca-1* suppress the locomotion defect of animals expressing activated Rho. (A) Animals expressing an activated Rho mutant (G14V) in acetylcholine neurons (*nzls29* transgene, written as Rho*) have a slow locomotion rate as measured by the number of

body bends. The *nlf-1(ox327)* and *nca-1(gk9)* mutations, but not *nca-2(gk5)*, strongly suppress the slow locomotion rate of activated Rho. The wild-type data shown in the right graph are the same as shown in Figure 3E, left graph. (B) Animals expressing an activated Rho mutant (G14V) in acetylcholine neurons (*Rho**) have reduced locomotion as measured in radial locomotion assays. Mutations that eliminate function of the NCA channels (*unc-80(ox330)* or *nca-2(gk5)*; *nca-1(gk9)*) increase the radial distance traveled by activated Rho mutants, but the effect is subtle since *unc-80* and *nca-2*; *nca-1* mutants have reduced locomotion on their own. The *nlf-1(ox327)* mutation that partially reduces function of the NCA channels strongly suppresses the locomotion defect of activated Rho. In the particular radial locomotion experiment shown here, only five *Rho**; *nca-1* animals were assayed and they had a mean radial distance traveled of 2.4 mm, very similar to the mean radial distance of the *Rho** single mutant (2.0 mm, n=18). However, in an independent experiment, the *Rho**; *nca-1* double mutant had a mean radial distance of 12.2 mm (n=10) as compared to 3.5 mm for the *Rho** single mutant (n=10). Thus, it is likely that *nca-1* does indeed suppress *Rho** in radial locomotion assays, but gave a negative result in the presented assay due to low n, with the likely explanation that these particular *Rho**; *nca-1* animals moved outward and returned to the center. ***, P<0.001; ns, not significant, P>0.05, Bonferroni test. Error bars = SEM; n = 10-16 (panel A); n = 5-18 (panel B).

Figure 8 Mutations in NCA channel subunits suppress the high-amplitude waveform and locomotion of adult animals expressing activated Rho. Animals expressing an activated Rho mutant (G14V) only in adults by heat-shock induced expression (*nzIs1* transgene, *hs::Rho**) have a high-amplitude waveform. The *unc-80(ox330)* and *nlf-1(ox327)* mutations strongly suppress the high-amplitude waveform of activated Rho. *unc-80*, but not *nlf-1*, makes the activated Rho animals faint. (A) Photos of first-day adult worms. (B) Photos of worm tracks. (C) Quantification of track waveform. (D) Animals expressing an activated Rho mutant (G14V) only in adults by heat-shock

induced expression (*nzls1* transgene, *hs::Rho*^{*}) have a reduced locomotion rate. The *nlf-1(ox327)* mutation suppresses the reduced locomotion rate of activated Rho. Statistics in C: ***, P<0.001, Bonferroni test. Error bars = SEM; n = 5. Statistics in D: *, P=0.0157, two-tailed unpaired t test. Error bars = SEM; n = 18-30.

Figure 9 An activated NCA-1 mutant suppresses the straight posture and low-amplitude waveform of an activated GOA-1 mutant. The *goa-1(n499 ox304)* mutant (written as Go^{*}) has a strong movement defect as shown by a body bend assay (A) and a radial locomotion assay (B). ***, P<0.001; **, P<0.01, two-tailed unpaired t-tests. Error bars = SEM; n = 10 (panel A); n = 18 (panel B). Also the *goa-1(n499 ox304)* mutant has a relatively straight posture (C) and low-amplitude waveform (D) that is suppressed by the *nca-1(ox352)* mutation (written as Nca^{*}). The wild-type waveform data are the same data shown in Figures 2C, 3D, and 6C. ***, P<0.001; **, P<0.01, Bonferroni test. Comparisons are to Go^{*}. Error bars = SEM; n = 5-6.

Figure 10 Model. G_q activates NCA-1 in a linear pathway via the RhoGEF Trio and small G protein Rho. G_q activation of Trio and Rho is direct (solid arrow). Rho activation of the NCA-1 channel is likely to be indirect (dashed arrow). G_o inhibits G_q via the RGS protein EAT-16 (Hajdu-Cronin *et al.* 1999). Thus, loss-of-function mutations in the channel pore-forming subunit NCA-1, its associated subunits UNC-79 and UNC-80, or the ER-localized NCA channel assembly factor NLF-1 suppress an activated G_q mutant, whereas a gain-of-function activating mutation in NCA-1 suppresses an activated G_o mutant. Though the NCA-1 channel has the greatest role in conveying G_q-Rho signals, channels composed of the NCA-2 pore-forming subunit are also probably regulated by G_q because elimination of both NCA-1 and NCA-2 is required to fully suppress activated G_q and activated Rho mutants.

Figure S1 *nlf-1* mutants have reduced *nca-1::gfp* and *nca-2::gfp* fluorescence in the nerve ring. Quantification of the nerve ring fluorescence of C-terminally tagged *nca-1::gfp* (transgene *vals46*) and *nca-2::gfp* (transgene *vals41*) in wild type and *nlf-1(ox327)* mutants. ***, $P < 0.001$, two-tailed unpaired t tests where each mutant strain is compared to its associated wild-type control. Error bars = SEM; $n = 11-12$.

Literature Cited

Adachi T., Kunitomo H., Tomioka M., Ohno H., Okochi Y. *et al.*, 2010 Reversal of salt preference is directed by the insulin/PI3K and Gq/PKC signaling in *Caenorhabditis elegans*. *Genetics* **186**: 1309–1319.

Ailion M., Hannemann M., Dalton S., Pappas A., Watanabe S. *et al.*, 2014 Two Rab2 interactors regulate dense-core vesicle maturation. *Neuron* **82**: 167–180.

Aktories K., Wilde C., Vogelsang M., 2004 Rho-modifying C3-like ADP-ribosyltransferases. *Rev. Physiol. Biochem. Pharmacol.* **152**: 1–22.

Al-Sayed M. D., Al-Zaidan H., Albakheet A., Hakami H., Kenana R. *et al.*, 2013 Mutations in NALCN cause an autosomal-recessive syndrome with severe hypotonia, speech impairment, and cognitive delay. *Am. J. Hum. Genet.* **93**: 721–726.

Aoyagi K., Rossignol E., Hamdan F. F., Mulcahy B., Xie L. *et al.*, 2015 A Gain-of-Function Mutation in NALCN in a Child with Intellectual Disability, Ataxia, and Arthrogryposis. *Hum. Mutat.* **36**: 753–757.

Balla T., 2013 Phosphoinositides: tiny lipids with giant impact on cell regulation. *Physiol. Rev.* **93**: 1019–1137.

- 793 Bastiani C. A., Gharib S., Simon M. I., Sternberg P. W., 2003 *Caenorhabditis elegans* Gα_q
794 regulates egg-laying behavior via a PLCβ-independent and serotonin-dependent
795 signaling pathway and likely functions both in the nervous system and in muscle. *Genetics*
796 **165**: 1805–1822.
- 797 Bend E. G., Si Y., Stevenson D. A., Bayrak-Toydemir P., Newcomb T. M. *et al.*, 2016 NALCN
798 channelopathies: Distinguishing gain-of-function and loss-of-function mutations. *Neurology*
799 **87**: 1131–1139.
- 800 Boone A. N., Senatore A., Chemin J., Monteil A., Spafford J. D., 2014 Gd³⁺ and calcium
801 sensitive, sodium leak currents are features of weak membrane-glass seals in patch clamp
802 recordings. *PLoS ONE* **9**: e98808.
- 803 Bouhours M., Po M. D., Gao S., Hung W., Li H. *et al.*, 2011 A co-operative regulation of neuronal
804 excitability by UNC-7 innexin and NCA/NALCN leak channel. *Mol Brain* **4**: 16.
- 805 Brundage L., Avery L., Katz A., Kim U. J., Mendel J. E. *et al.*, 1996 Mutations in a *C. elegans*
806 Gα_q gene disrupt movement, egg laying, and viability. *Neuron* **16**: 999–1009.
- 807 Charlie N. K., Schade M. A., Thomure A. M., Miller K. G., 2006 Presynaptic UNC-31 (CAPS) is
808 required to activate the G α_q(s) pathway of the *Caenorhabditis elegans* synaptic
809 signaling network. *Genetics* **172**: 943–961.
- 810 Chatah N. E., Abrams C. S., 2001 G-protein-coupled receptor activation induces the membrane
811 translocation and activation of phosphatidylinositol-4-phosphate 5-kinase I α by a Rac-
812 and Rho-dependent pathway. *J. Biol. Chem.* **276**: 34059–34065.

- 813 Chong J. X., McMillin M. J., Shively K. M., Beck A. E., Marvin C. T. *et al.*, 2015 De novo mutations
814 in NALCN cause a syndrome characterized by congenital contractures of the limbs and
815 face, hypotonia, and developmental delay. *Am. J. Hum. Genet.* **96**: 462–473.
- 816 Coleman D. E., Berghuis A. M., Lee E., Linder M. E., Gilman A. G. *et al.*, 1994 Structures of active
817 conformations of Gi alpha 1 and the mechanism of GTP hydrolysis. *Science* **265**: 1405–
818 1412.
- 819 Coulon P., Kanyshkova T., Broicher T., Munsch T., Wettschureck N. *et al.*, 2010 Activity Modes in
820 Thalamocortical Relay Neurons are Modulated by G(q)/G(11) Family G-proteins -
821 Serotonergic and Glutamatergic Signaling. *Front Cell Neurosci* **4**: 132.
- 822 Davis M. W., Hammarlund M., Harrach T., Hullett P., Olsen S. *et al.*, 2005 Rapid single nucleotide
823 polymorphism mapping in *C. elegans*. *BMC Genomics* **6**: 118.
- 824 Davis M. W., Morton J. J., Carroll D., Jorgensen E. M., 2008 Gene activation using FLP
825 recombinase in *C. elegans*. *PLoS Genet.* **4**: e1000028.
- 826 Esposito G., Amoroso M. R., Bergamasco C., Di Schiavi E., Bazzicalupo P., 2010 The G protein
827 regulators EGL-10 and EAT-16, the G α GOA-1 and the G(q) α EGL-30 modulate the
828 response of the *C. elegans* ASH polymodal nociceptive sensory neurons to repellents.
829 *BMC Biol.* **8**: 138.
- 830 Etienne-Manneville S., Hall A., 2002 Rho GTPases in cell biology. *Nature* **420**: 629–635.
- 831 Fukai R., Saitsu H., Okamoto N., Sakai Y., Fattal-Valevski A. *et al.*, 2016 De novo missense
832 mutations in NALCN cause developmental and intellectual impairment with hypotonia. *J.*
833 *Hum. Genet.* **61**: 451–455.

- 834 Funato H., Miyoshi C., Fujiyama T., Kanda T., Sato M. *et al.*, 2016 Forward-genetics analysis of
835 sleep in randomly mutagenized mice. *Nature* **539**: 378–383.
- 836 Gal M., Magen D., Zahran Y., Ravid S., Eran A. *et al.*, 2016 A novel homozygous splice site
837 mutation in NALCN identified in siblings with cachexia, strabismus, severe intellectual
838 disability, epilepsy and abnormal respiratory rhythm. *Eur J Med Genet* **59**: 204–209.
- 839 Gamper N., Reznikov V., Yamada Y., Yang J., Shapiro M. S., 2004 Phosphatidylinositol 4,5-
840 bisphosphate signals underlie receptor-specific Gq/11-mediated modulation of N-type Ca²⁺
841 channels. *J. Neurosci.* **24**: 10980–10992.
- 842 Gao S., Xie L., Kawano T., Po M. D., Pirri J. K. *et al.*, 2015 The NCA sodium leak channel is
843 required for persistent motor circuit activity that sustains locomotion. *Nat Commun* **6**: 6323.
- 844 Hajdu-Cronin Y. M., Chen W. J., Patikoglou G., Koelle M. R., Sternberg P. W., 1999 Antagonism
845 between G(o)alpha and G(q)alpha in *Caenorhabditis elegans*: the RGS protein EAT-16 is
846 necessary for G(o)alpha signaling and regulates G(q)alpha activity. *Genes Dev* **13**: 1780–
847 1793.
- 848 Hajdu-Cronin Y. M., Chen W. J., Sternberg P. W., 2004 The L-type cyclin CYL-1 and the heat-
849 shock-factor HSF-1 are required for heat-shock-induced protein expression in
850 *Caenorhabditis elegans*. *Genetics* **168**: 1937–1949.
- 851 Hammarlund M., Palfreyman M. T., Watanabe S., Olsen S., Jorgensen E. M., 2007 Open syntaxin
852 docks synaptic vesicles. *PLoS Biol.* **5**: e198.
- 853 Hiley E., McMullan R., Nurrish S. J., 2006 The Galpha12-RGS RhoGEF-RhoA signalling pathway
854 regulates neurotransmitter release in *C. elegans*. *EMBO J.* **25**: 5884–5895.

- 855 Humphrey J. A., Hamming K. S., Thacker C. M., Scott R. L., Sedensky M. M. *et al.*, 2007 A
856 putative cation channel and its novel regulator: cross-species conservation of effects on
857 general anesthesia. *Curr. Biol.* **17**: 624–629.
- 858 Jaffe A. B., Hall A., 2005 Rho GTPases: biochemistry and biology. *Annu. Rev. Cell Dev. Biol.* **21**:
859 247–269.
- 860 Jantsch-Plunger V., Gönczy P., Romano A., Schnabel H., Hamill D. *et al.*, 2000 CYK-4: A Rho
861 family gtpase activating protein (GAP) required for central spindle formation and
862 cytokinesis. *J. Cell Biol.* **149**: 1391–1404.
- 863 Jospin M., Watanabe S., Joshi D., Young S., Hamming K. *et al.*, 2007 UNC-80 and the NCA ion
864 channels contribute to endocytosis defects in synaptojanin mutants. *Curr. Biol.* **17**: 1595–
865 1600.
- 866 Just I., Mohr C., Schallehn G., Menard L., Didsbury J. R. *et al.*, 1992 Purification and
867 characterization of an ADP-ribosyltransferase produced by *Clostridium limosum*. *J. Biol.*
868 *Chem.* **267**: 10274–10280.
- 869 Karakaya M., Heller R., Kunde V., Zimmer K.-P., Chao C.-M. *et al.*, 2016 Novel Mutations in the
870 Nonselective Sodium Leak Channel (NALCN) Lead to Distal Arthrogryposis with Increased
871 Muscle Tone. *Neuropediatrics* **47**:273-277.
- 872 Kasap M., Bonnett K., Aamodt E. J., Dwyer D. S., 2017 Akinesia and freezing caused by Na(+)
873 leak-current channel (NALCN) deficiency corrected by pharmacological inhibition of K(+)
874 channels and gap junctions. *J. Comp. Neurol.* **525**: 1109–1121.
- 875 Köroğlu Ç., Seven M., Tolun A., 2013 Recessive truncating NALCN mutation in infantile
876 neuroaxonal dystrophy with facial dysmorphism. *J. Med. Genet.* **50**: 515–520.

877 Krause M., Offermanns S., Stocker M., Pedarzani P., 2002 Functional specificity of G alpha q and
878 G alpha 11 in the cholinergic and glutamatergic modulation of potassium currents and
879 excitability in hippocampal neurons. *J. Neurosci.* **22**: 666–673.

880 Lackner M. R., Nurrish S. J., Kaplan J. M., 1999 Facilitation of synaptic transmission by EGL-30
881 Gqalpha and EGL-8 PLCbeta: DAG binding to UNC-13 is required to stimulate
882 acetylcholine release. *Neuron* **24**: 335–346.

883 Lear B. C., Lin J.-M., Keath J. R., McGill J. J., Raman I. M. *et al.*, 2005 The ion channel narrow
884 abdomen is critical for neural output of the Drosophila circadian pacemaker. *Neuron* **48**:
885 965–976.

886 Lear B. C., Darrah E. J., Aldrich B. T., Gebre S., Scott R. L. *et al.*, 2013 UNC79 and UNC80,
887 Putative Auxiliary Subunits of the NARROW ABDOMEN Ion Channel, Are Indispensable for
888 Robust Circadian Locomotor Rhythms in Drosophila. *PLoS ONE* **8**: e78147.

889 Lee J. H., Cribbs L. L., Perez-Reyes E., 1999 Cloning of a novel four repeat protein related to
890 voltage-gated sodium and calcium channels. *FEBS Lett.* **445**: 231–236.

891 Liebeskind B. J., Hillis D. M., Zakon H. H., 2012 Phylogeny unites animal sodium leak channels
892 with fungal calcium channels in an ancient, voltage-insensitive clade. *Mol. Biol. Evol.* **29**:
893 3613–3616.

894 Littleton J. T., Ganetzky B., 2000 Ion channels and synaptic organization: analysis of the
895 Drosophila genome. *Neuron* **26**: 35–43.

896 Lozic B., Johansson S., Lovric Kojundzic S., Markic J., Knappskog P. M. *et al.*, 2016 Novel
897 NALCN variant: altered respiratory and circadian rhythm, anesthetic sensitivity. *Ann Clin*
898 *Transl Neurol* **3**: 876–883.

- 899 Lu B., Su Y., Das S., Liu J., Xia J. *et al.*, 2007 The neuronal channel NALCN contributes resting
900 sodium permeability and is required for normal respiratory rhythm. *Cell* **129**: 371–383.
- 901 Lu B., Su Y., Das S., Wang H., Wang Y. *et al.*, 2009 Peptide neurotransmitters activate a cation
902 channel complex of NALCN and UNC-80. *Nature* **457**: 741–744.
- 903 Lu B., Zhang Q., Wang H., Wang Y., Nakayama M. *et al.*, 2010 Extracellular calcium controls
904 background current and neuronal excitability via an UNC79-UNC80-NALCN cation channel
905 complex. *Neuron* **68**: 488–499.
- 906 Lu T. Z., Feng Z.-P., 2011 A sodium leak current regulates pacemaker activity of adult central
907 pattern generator neurons in *Lymnaea stagnalis*. *PLoS ONE* **6**: e18745.
- 908 Lutas A., Lahmann C., Soumillon M., Yellen G., 2016 The leak channel NALCN controls tonic
909 firing and glycolytic sensitivity of substantia nigra pars reticulata neurons. *eLife* **5**: e15271.
- 910 Lutz S., Freichel-Blomquist A., Yang Y., Rümenapp U., Jakobs K. H. *et al.*, 2005 The guanine
911 nucleotide exchange factor p63RhoGEF, a specific link between Gq/11-coupled receptor
912 signaling and RhoA. *J. Biol. Chem.* **280**: 11134–11139.
- 913 Lutz S., Shankaranarayanan A., Coco C., Ridilla M., Nance M. R. *et al.*, 2007 Structure of
914 Galphaq-p63RhoGEF-RhoA complex reveals a pathway for the activation of RhoA by
915 GPCRs. *Science* **318**: 1923–1927.
- 916 Matsuki M., Kunitomo H., Iino Y., 2006 Gαq regulates olfactory adaptation by antagonizing
917 Gαq-DAG signaling in *Caenorhabditis elegans*. *Proc. Natl. Acad. Sci. U.S.A.* **103**:
918 11112–11117.
- 919 McMullan R., Hiley E., Morrison P., Nurrish S. J., 2006 Rho is a presynaptic activator of
920 neurotransmitter release at pre-existing synapses in *C. elegans*. *Genes Dev.* **20**: 65–76.

921 Mello C. C., Kramer J. M., Stinchcomb D., Ambros V., 1991 Efficient gene transfer in *C.elegans*:
 922 extrachromosomal maintenance and integration of transforming sequences. *EMBO J* **10**:
 923 3959–3970.

924 Mendel J. E., Korswagen H. C., Liu K. S., Hajdu-Cronin Y. M., Simon M. I. *et al.*, 1995
 925 Participation of the protein Go in multiple aspects of behavior in *C. elegans*. *Science* **267**:
 926 1652–1655.

927 Miller K. G., Emerson M. D., Rand J. B., 1999 Gqalpha and diacylglycerol kinase negatively
 928 regulate the Gqalpha pathway in *C. elegans*. *Neuron* **24**: 323–333.

929 Morgan P. G., Sedensky M. M., 1995 Mutations affecting sensitivity to ethanol in the nematode,
 930 *Caenorhabditis elegans*. *Alcohol. Clin. Exp. Res.* **19**: 1423–1429.

931 Park E. C., Horvitz H. R., 1986 Mutations with dominant effects on the behavior and morphology
 932 of the nematode *Caenorhabditis elegans*. *Genetics* **113**: 821–852.

933 Pereira L., Kratsios P., Serrano-Saiz E., Sheftel H., Mayo A. E. *et al.*, 2015 A cellular and
 934 regulatory map of the cholinergic nervous system of *C. elegans*. *eLife* **4**: e12432.

935 Perez Y., Kadir R., Volodarsky M., Noyman I., Flusser H. *et al.*, 2016 UNC80 mutation causes a
 936 syndrome of hypotonia, severe intellectual disability, dyskinesia and dysmorphism, similar
 937 to that caused by mutations in its interacting cation channel NALCN. *J. Med. Genet.* **53**:
 938 397–402.

939 Pierce-Shimomura J. T., Chen B. L., Mun J. J., Ho R., Sarkis R. *et al.*, 2008 Genetic analysis of
 940 crawling and swimming locomotory patterns in *C. elegans*. *Proc. Natl. Acad. Sci. U.S.A.*
 941 **105**: 20982–20987.

- 942 Sánchez-Fernández G., Cabezudo S., García-Hoz C., Benincá C., Aragay A. M. *et al.*, 2014 Gαq
943 signalling: the new and the old. *Cell. Signal.* **26**: 833–848.
- 944 Sedensky M. M., Meneely P. M., 1987 Genetic analysis of halothane sensitivity in *Caenorhabditis*
945 *elegans*. *Science* **236**: 952–954.
- 946 Ségalat L., Elkes D. A., Kaplan J. M., 1995 Modulation of serotonin-controlled behaviors by Go in
947 *Caenorhabditis elegans*. *Science* **267**: 1648–1651.
- 948 Senatore A., Monteil A., Minnen J. van, Smit A. B., Spafford J. D., 2013 NALCN ion channels
949 have alternative selectivity filters resembling calcium channels or sodium channels. *PLoS*
950 *ONE* **8**: e55088.
- 951 Senatore A., Spafford J. D., 2013 A uniquely adaptable pore is consistent with NALCN being an
952 ion sensor. *Channels* **7**: 60–68.
- 953 Shamseldin H. E., Fageih E., Alasmari A., Zaki M. S., Gleeson J. G. *et al.*, 2016 Mutations in
954 UNC80, Encoding Part of the UNC79-UNC80-NALCN Channel Complex, Cause
955 Autosomal-Recessive Severe Infantile Encephalopathy. *Am. J. Hum. Genet.* **98**: 210–215.
- 956 Spencer A. G., Orita S., Malone C. J., Han M., 2001 A RHO GTPase-mediated pathway is
957 required during P cell migration in *Caenorhabditis elegans*. *Proc. Natl. Acad. Sci. U.S.A.*
958 **98**: 13132–13137.
- 959 Stray-Pedersen A., Cobben J.-M., Prescott T. E., Lee S., Cang C. *et al.*, 2016 Biallelic Mutations
960 in UNC80 Cause Persistent Hypotonia, Encephalopathy, Growth Retardation, and Severe
961 Intellectual Disability. *Am. J. Hum. Genet.* **98**: 202–209.

- 962 Swayne L. A., Mezghrani A., Varrault A., Chemin J., Bertrand G. *et al.*, 2009 The NALCN ion
963 channel is activated by M3 muscarinic receptors in a pancreatic beta-cell line. EMBO Rep.
964 **10**: 873–880.
- 965 Topalidou I., Cattin-Ortolá J., Pappas A. L., Cooper K., Merrihew G. E. *et al.*, 2016 The EARP
966 Complex and Its Interactor EIPR-1 Are Required for Cargo Sorting to Dense-Core Vesicles.
967 PLoS Genet. **12**: e1006074.
- 968 Valkanas E., Schaffer K., Dunham C., Maduro V., Souich C. du *et al.*, 2016 Phenotypic evolution
969 of UNC80 loss of function. Am. J. Med. Genet. A **170**: 3106–3114.
- 970 Vivero M., Cho M. T., Begtrup A., Wentzensen I. M., Walsh L. *et al.*, 2017 Additional de novo
971 missense genetic variants in NALCN associated with CLIFAHDD syndrome. Clin. Genet.
972 doi: **10.1111/cge.12899**.
- 973 Vogt S., Grosse R., Schultz G., Offermanns S., 2003 Receptor-dependent RhoA activation in
974 G12/G13-deficient cells: genetic evidence for an involvement of Gq/G11. J. Biol. Chem.
975 **278**: 28743–28749.
- 976 Wang Y., Koh K., Ichinose Y., Yasumura M., Ohtsuka T. *et al.*, 2016 A de novo mutation in the
977 NALCN gene in an adult patient with cerebellar ataxia associated with intellectual disability
978 and arthrogryposis. Clin. Genet. **90**: 556–557.
- 979 Weernink P. A. O., Meletiadis K., Hommeltenberg S., Hinz M., Ishihara H. *et al.*, 2004 Activation of
980 type I phosphatidylinositol 4-phosphate 5-kinase isoforms by the Rho GTPases, RhoA,
981 Rac1, and Cdc42. J. Biol. Chem. **279**: 7840–7849.

982 Wilkie T. M., Scherle P. A., Strathmann M. P., Slepak V. Z., Simon M. I., 1991 Characterization of
 983 G-protein alpha subunits in the Gq class: expression in murine tissues and in stromal and
 984 hematopoietic cell lines. *Proc. Natl. Acad. Sci. U.S.A.* **88**: 10049–10053.

985 Wilkie T. M., Gilbert D. J., Olsen A. S., Chen X. N., Amatruda T. T. *et al.*, 1992 Evolution of the
 986 mammalian G protein alpha subunit multigene family. *Nat. Genet.* **1**: 85–91.

987 Williams S. L., Lutz S., Charlie N. K., Vettel C., Ailion M. *et al.*, 2007 Trio's Rho-specific GEF
 988 domain is the missing Galpha q effector in *C. elegans*. *Genes Dev* **21**: 2731–2746.

989 Xie L., Gao S., Alcaire S. M., Aoyagi K., Wang Y. *et al.*, 2013 NLF-1 delivers a sodium leak
 990 channel to regulate neuronal excitability and modulate rhythmic locomotion. *Neuron* **77**:
 991 1069–1082.

992 Yeh E., Ng S., Zhang M., Bouhours M., Wang Y. *et al.*, 2008 A putative cation channel, NCA-1,
 993 and a novel protein, UNC-80, transmit neuronal activity in *C. elegans*. *PLoS Biol.* **6**: e55.

994

Figure 1

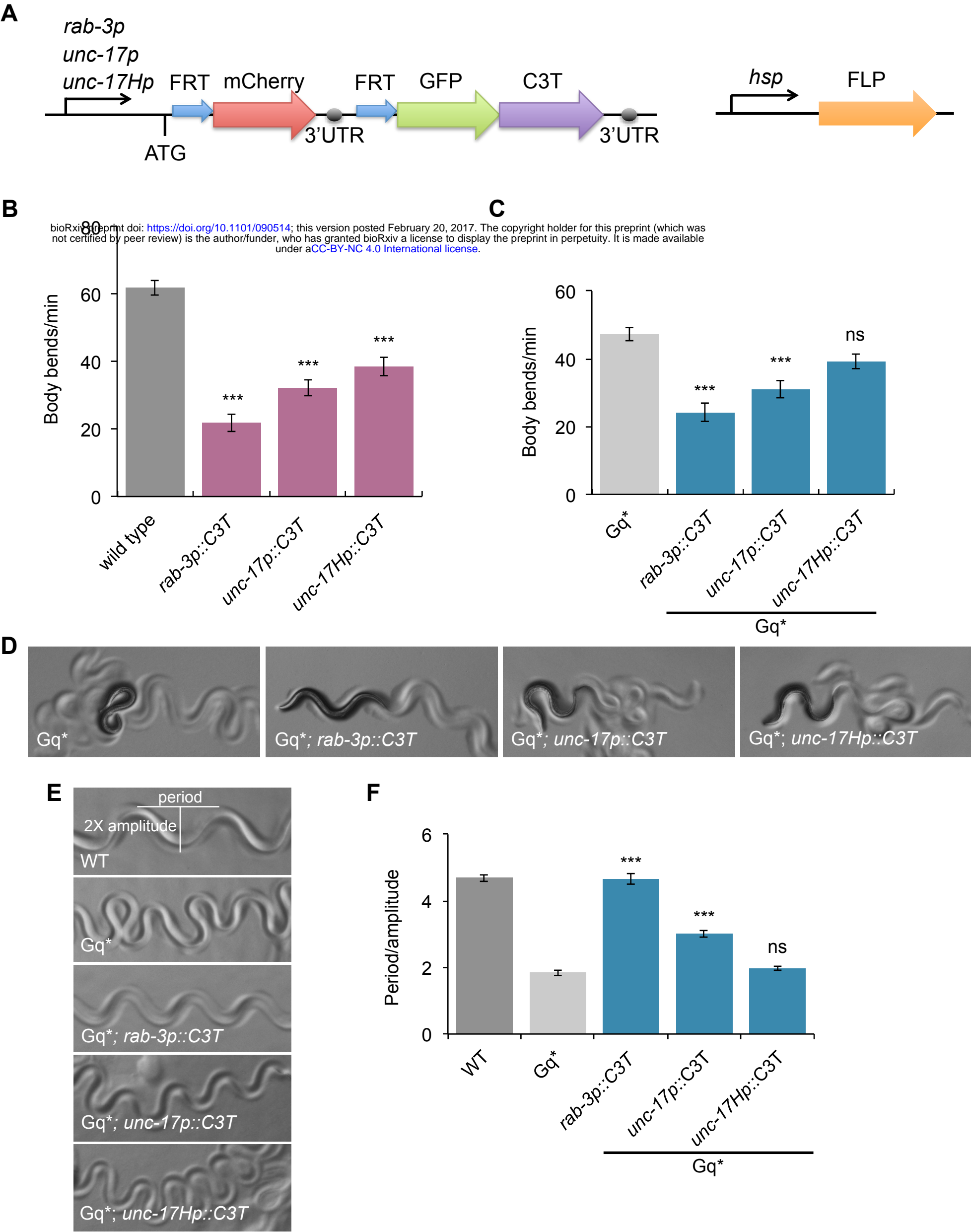
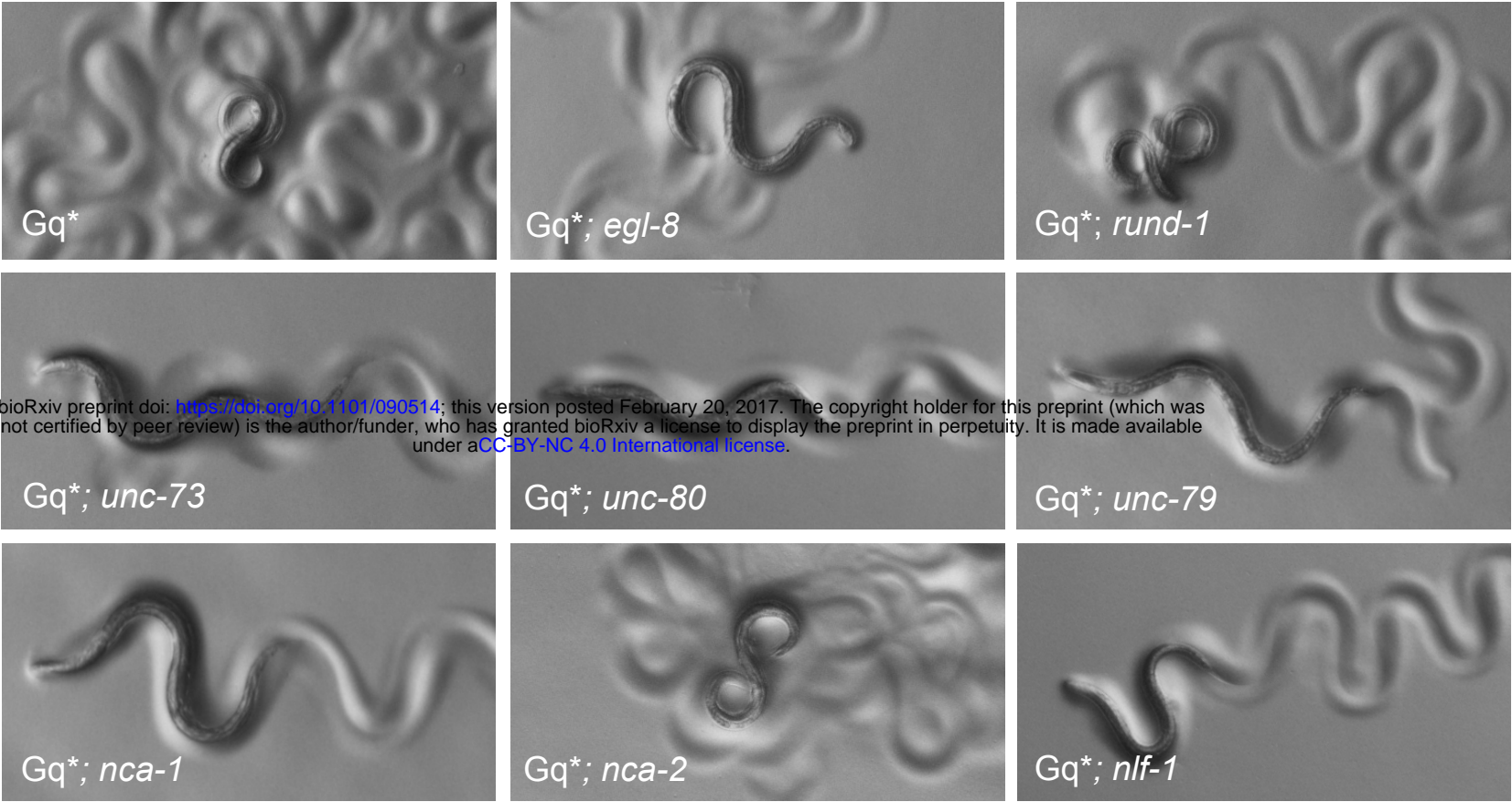
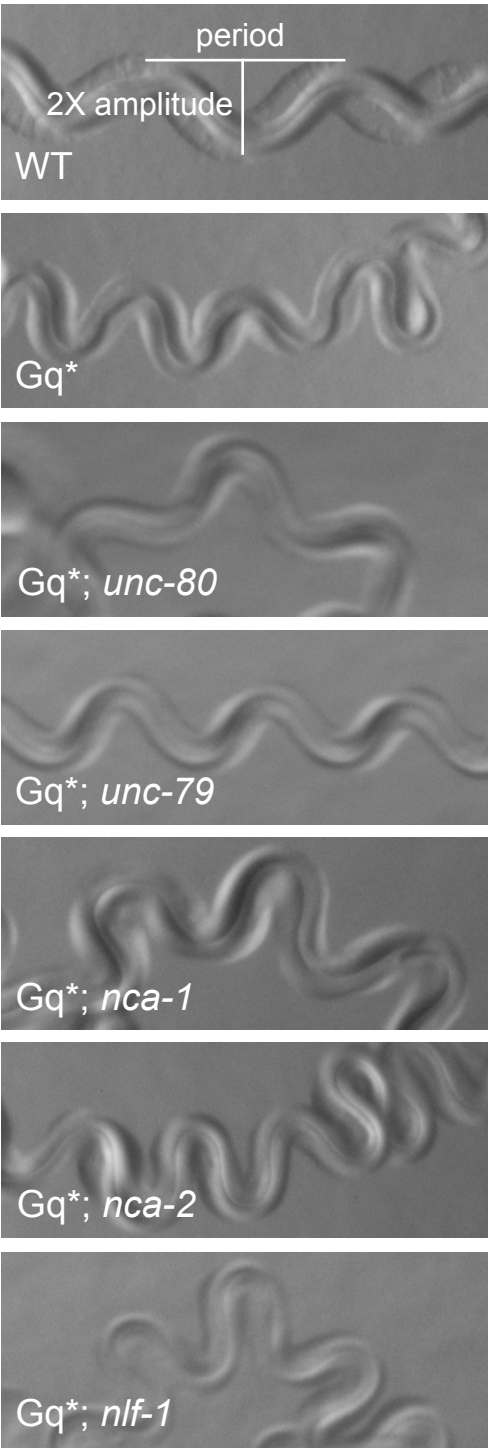


Figure 2

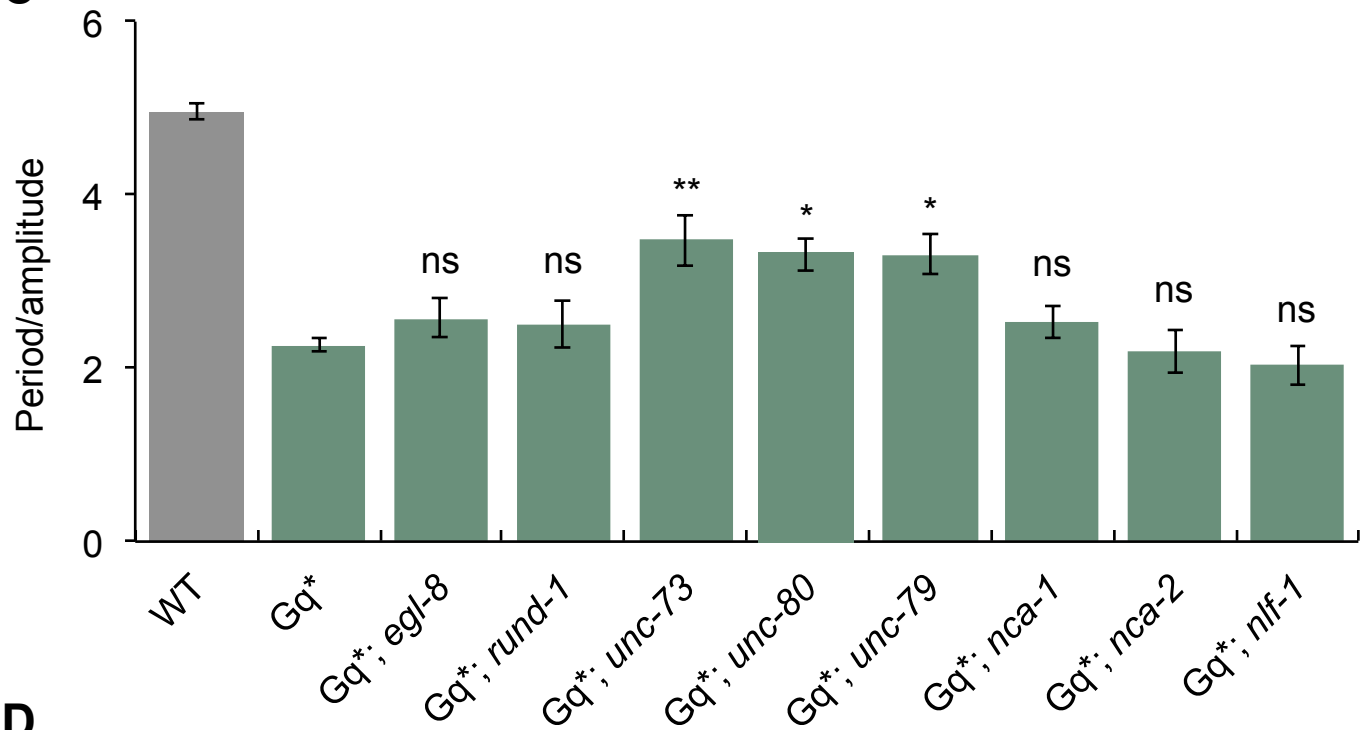
A



B



C



D

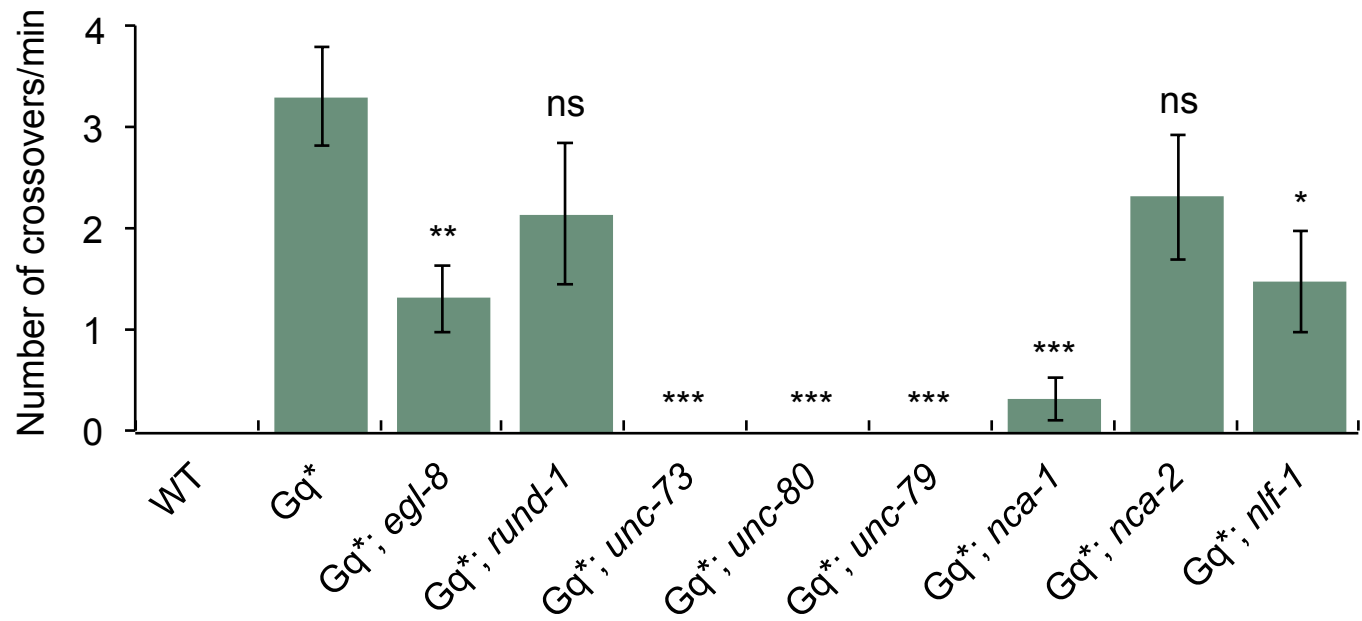


Figure 3

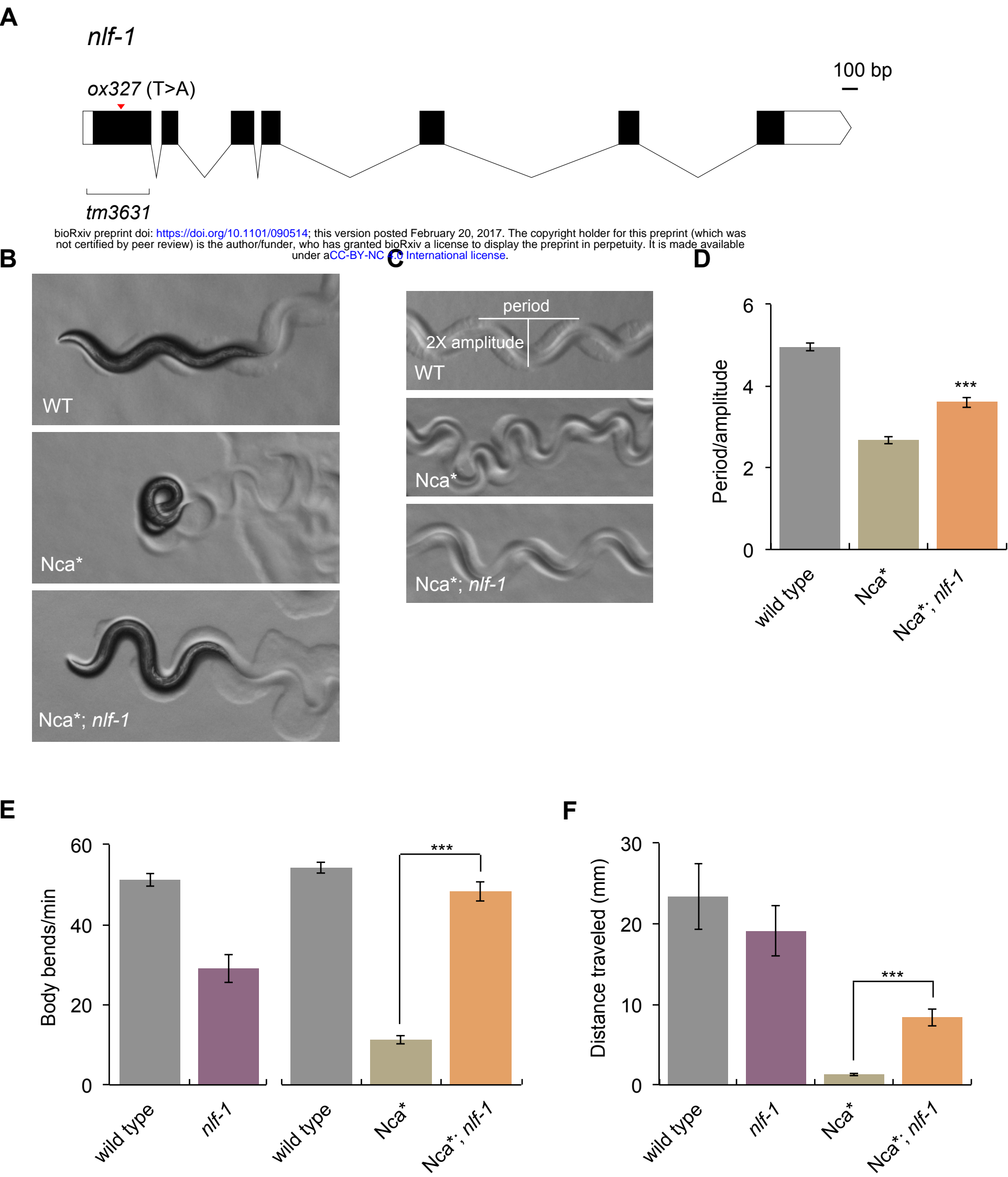
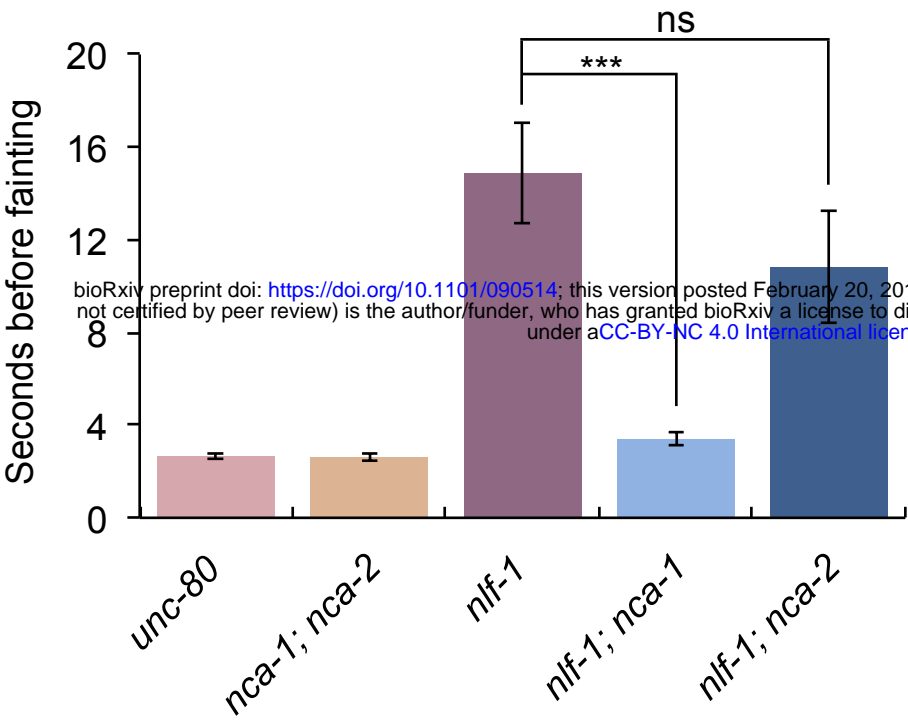


Figure 4

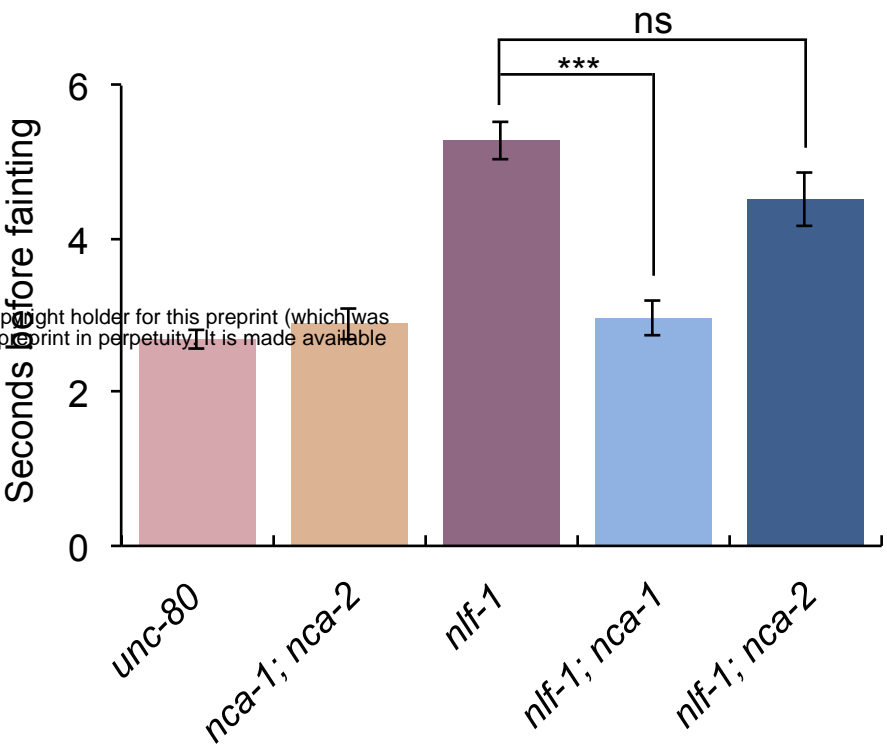
A

Forward



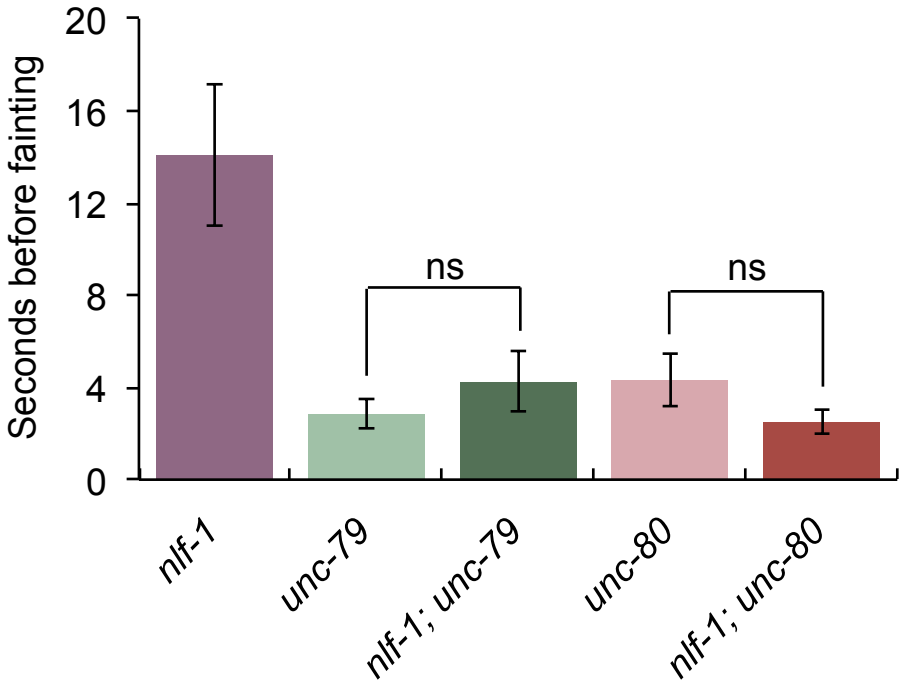
B

Backward



C

Forward



D

Backward

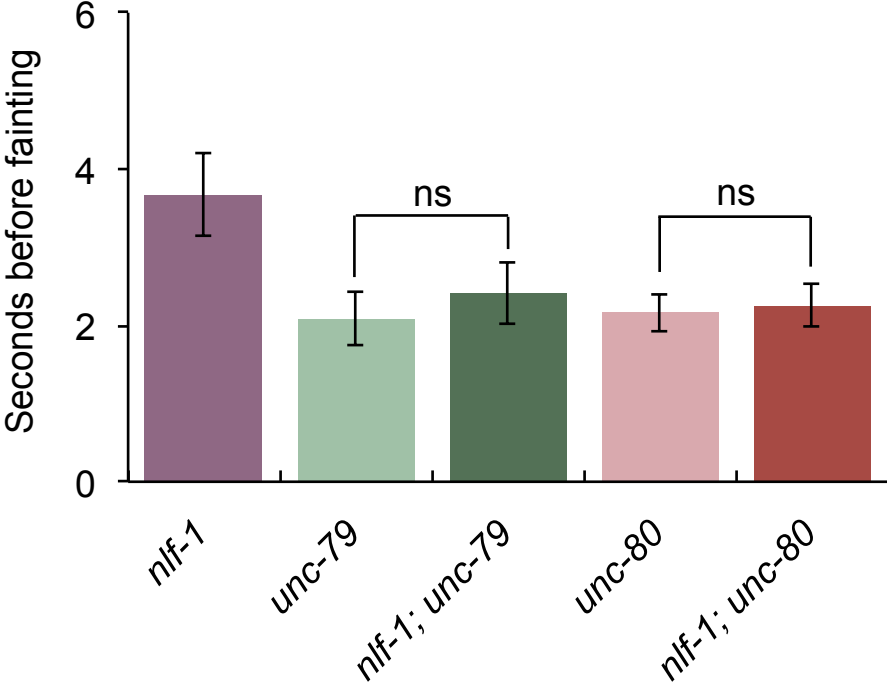
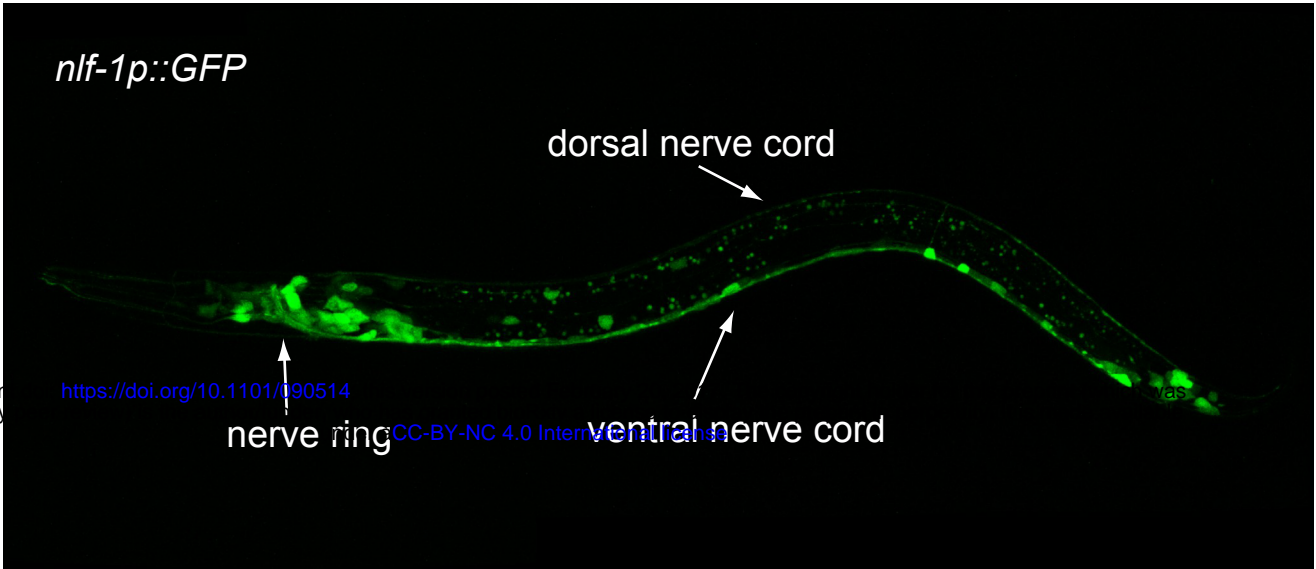
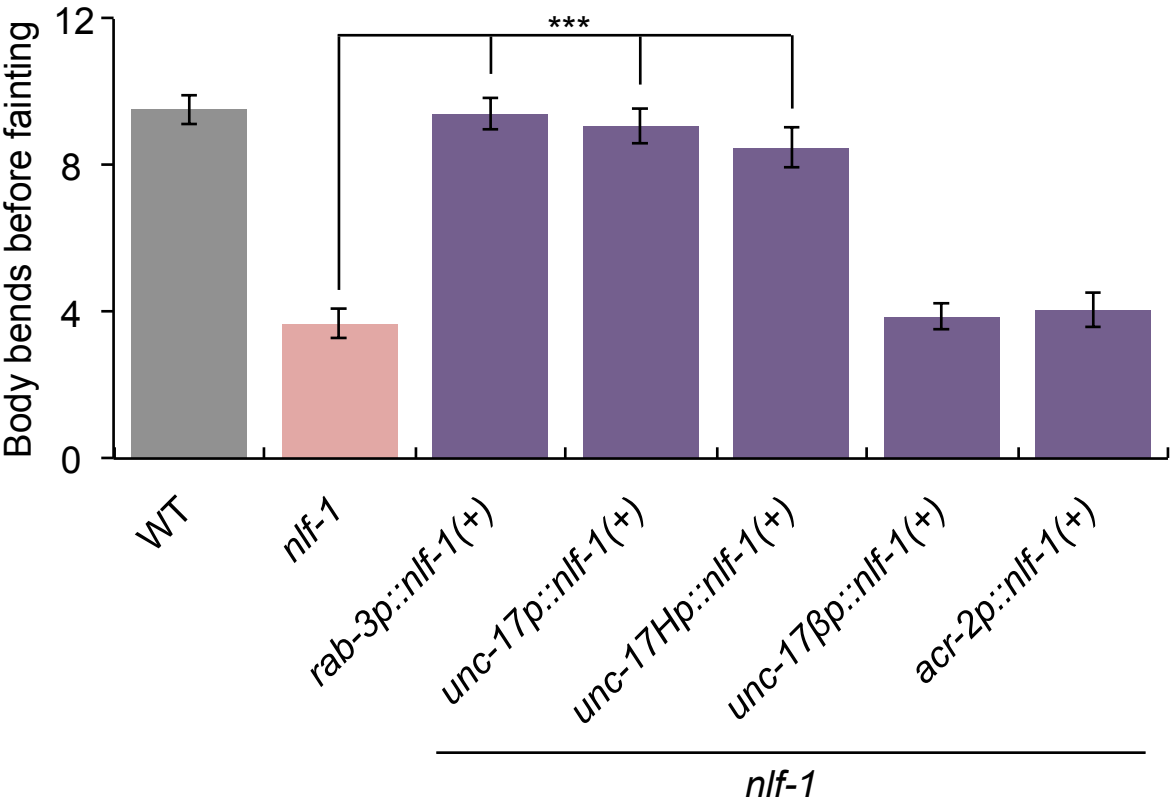


Figure 5

A



B



C

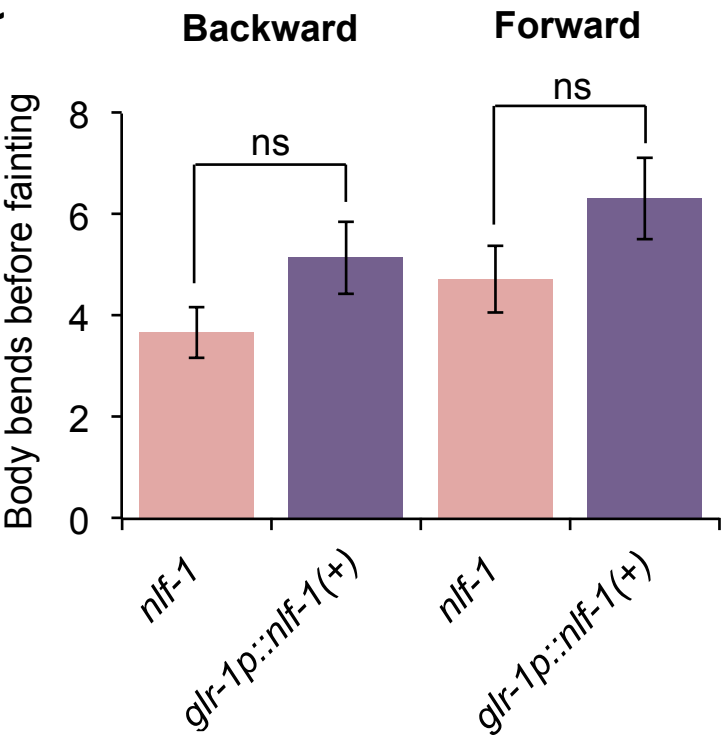
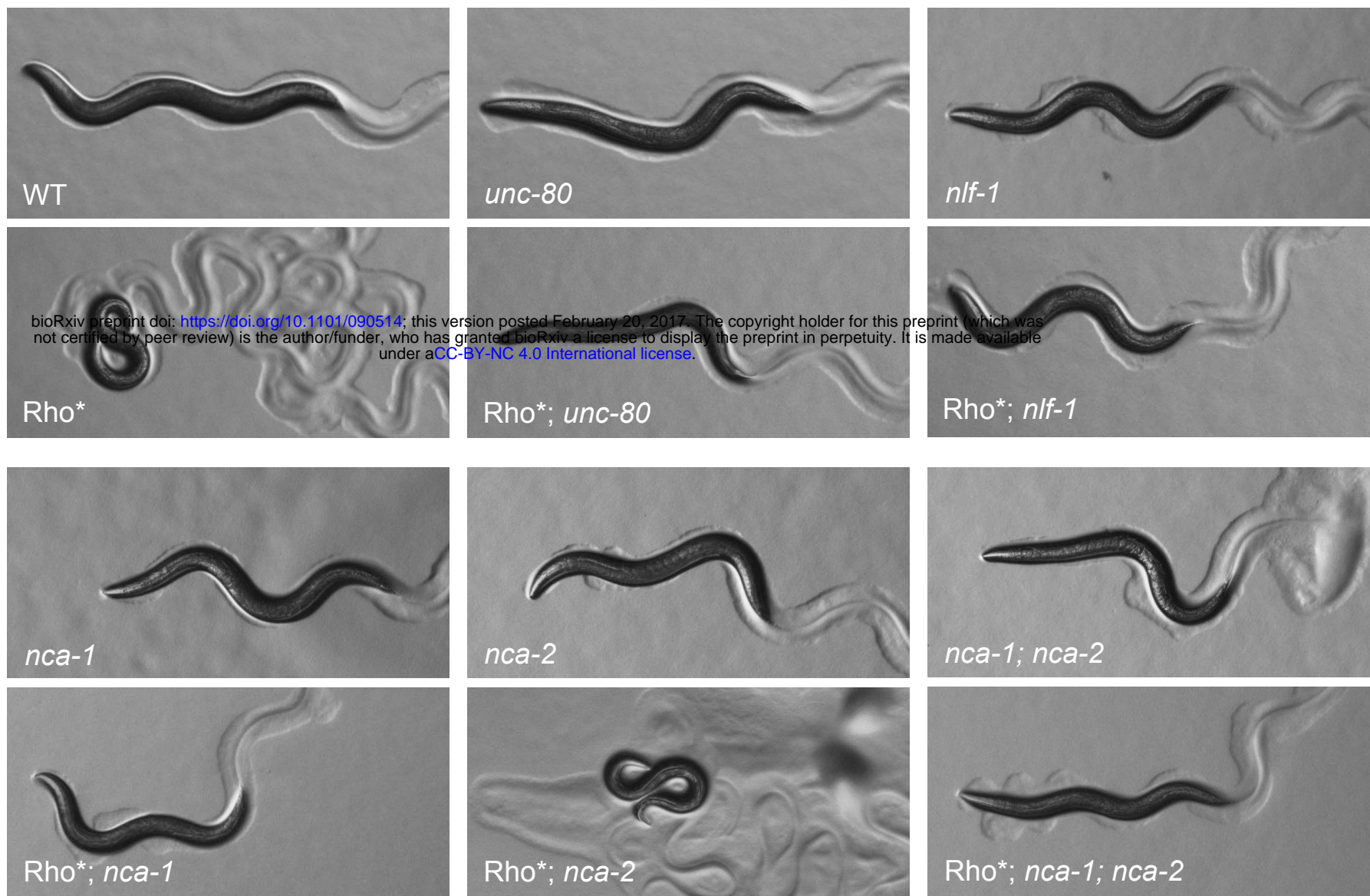
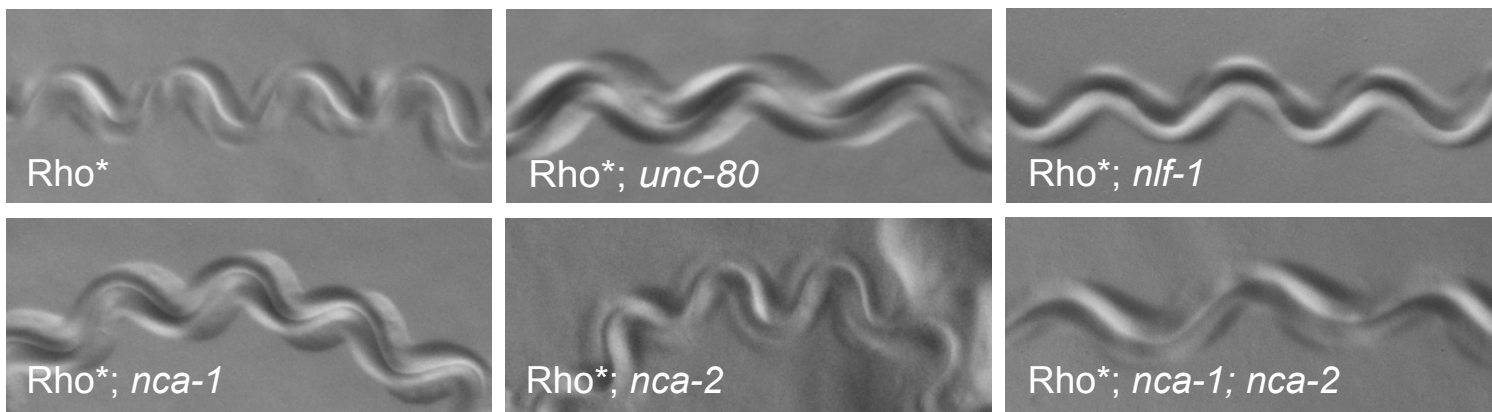


Figure 6

A



B



C

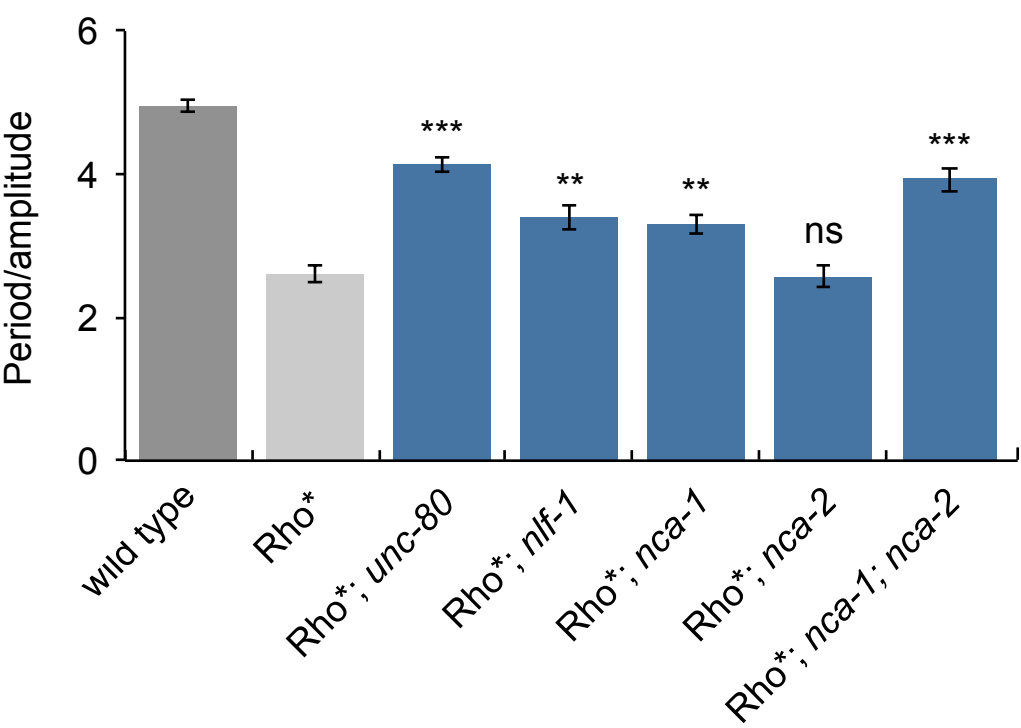


Figure 7

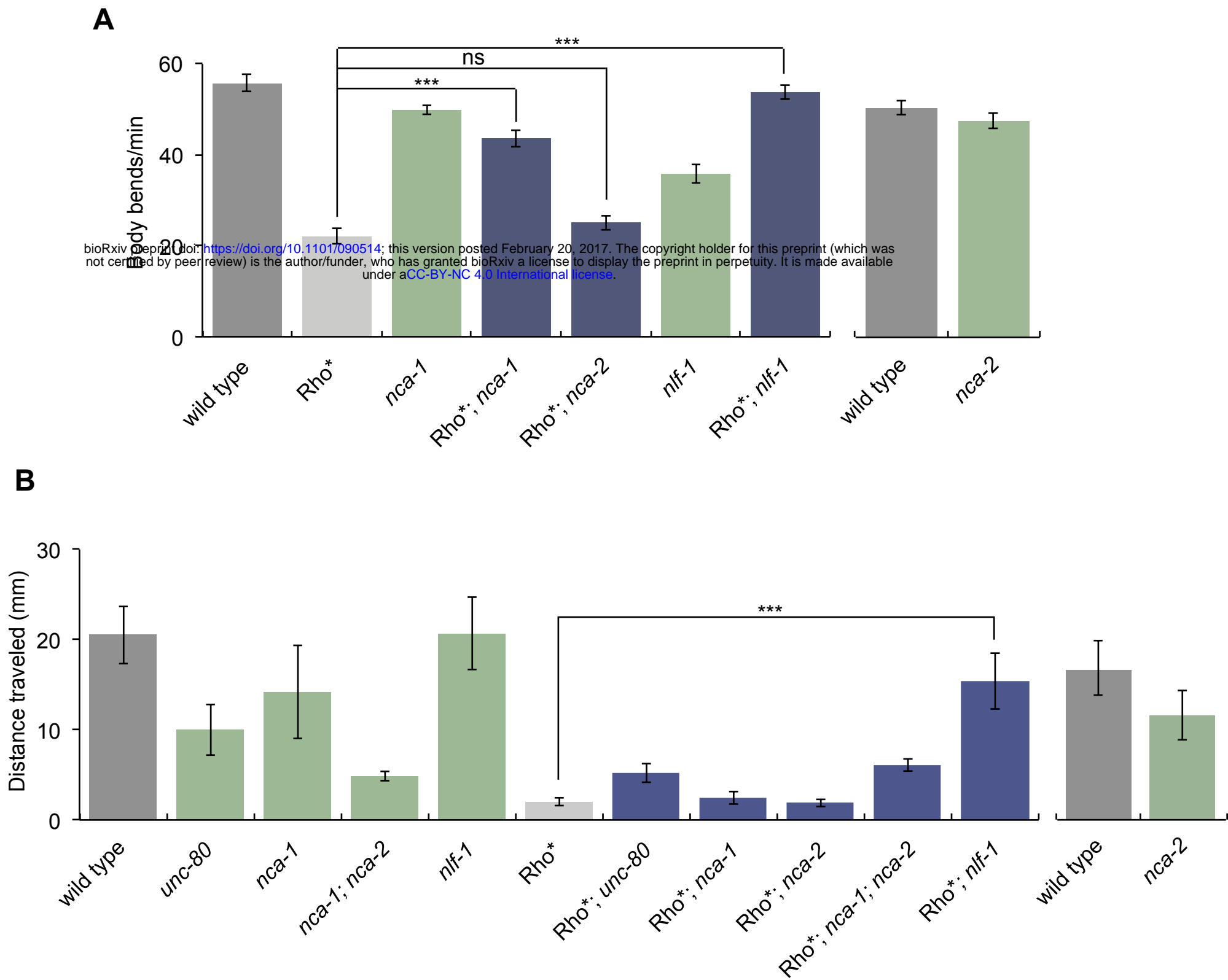
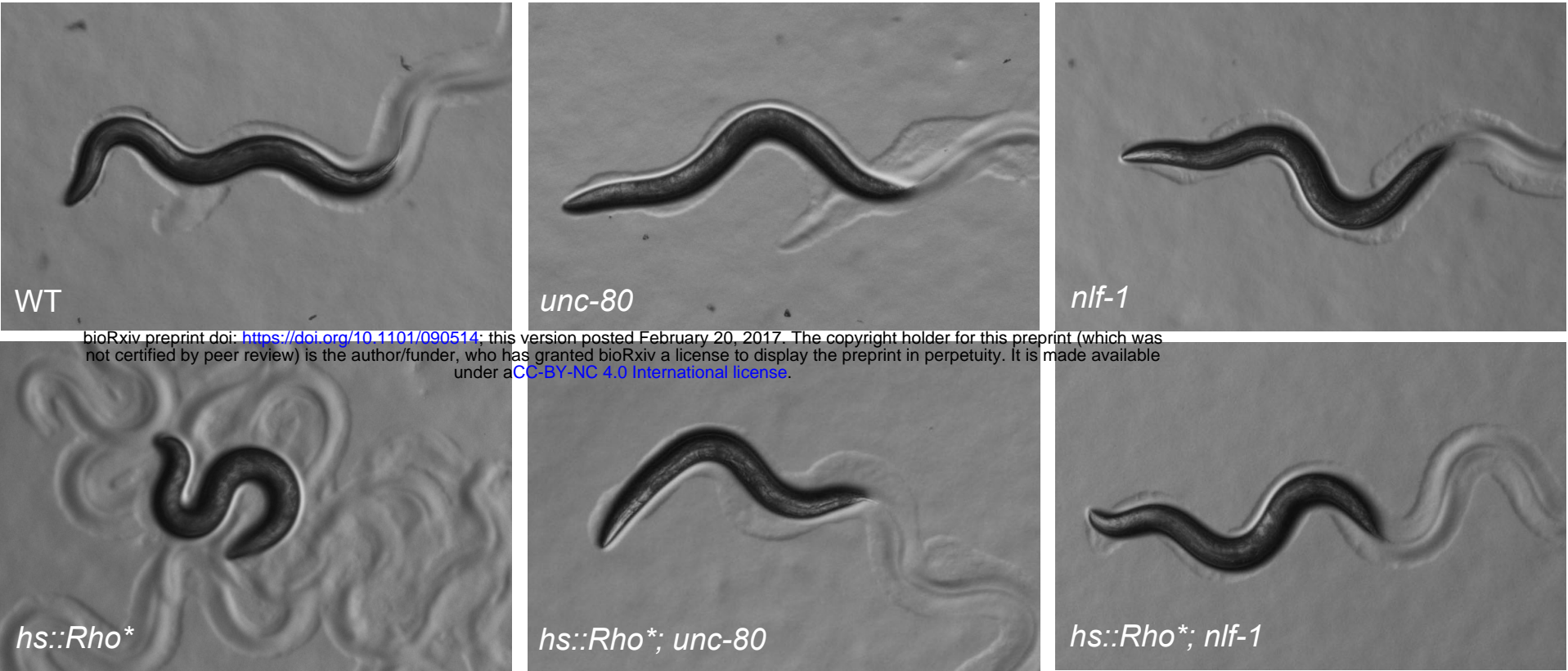
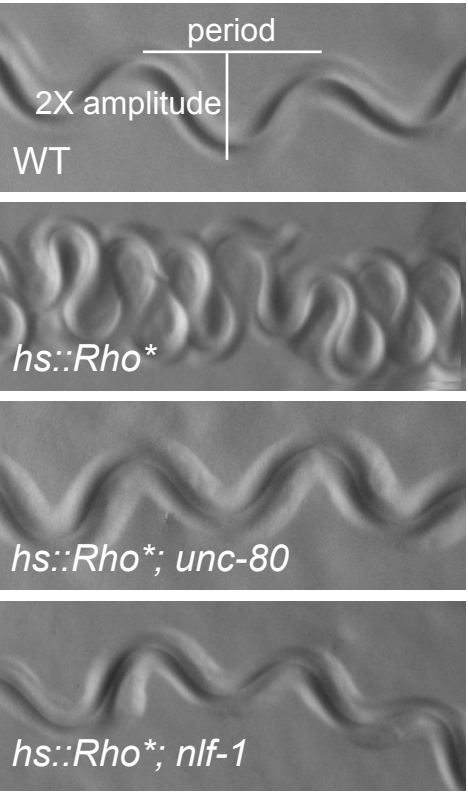


Figure 8

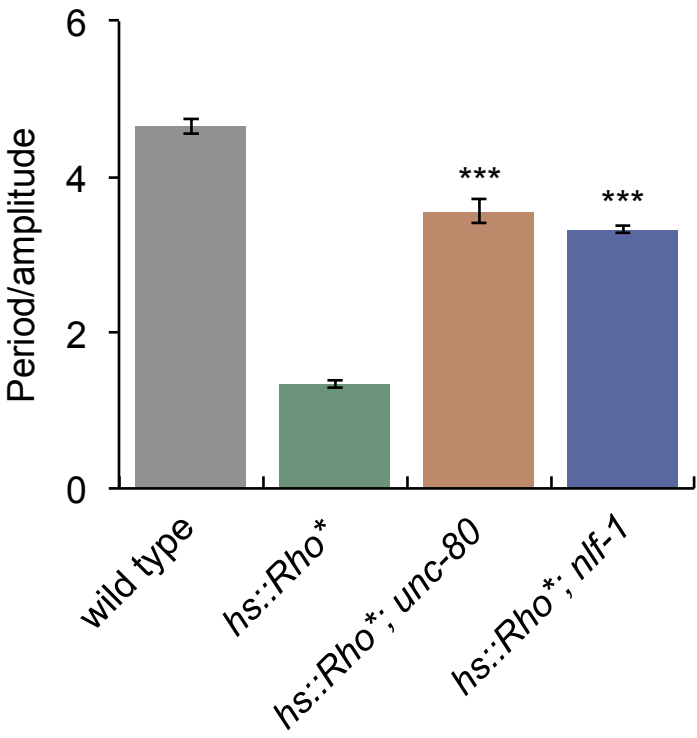
A



B



C



D

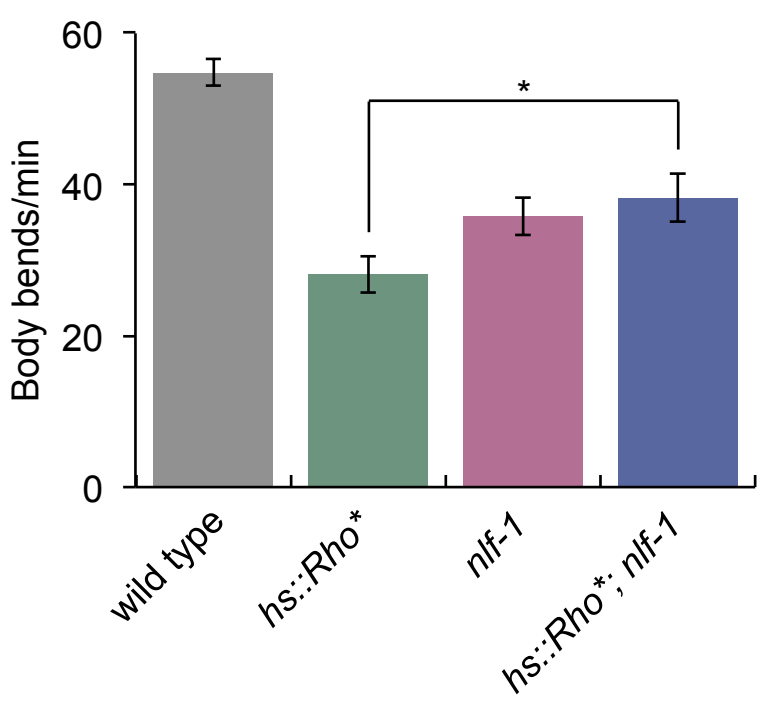
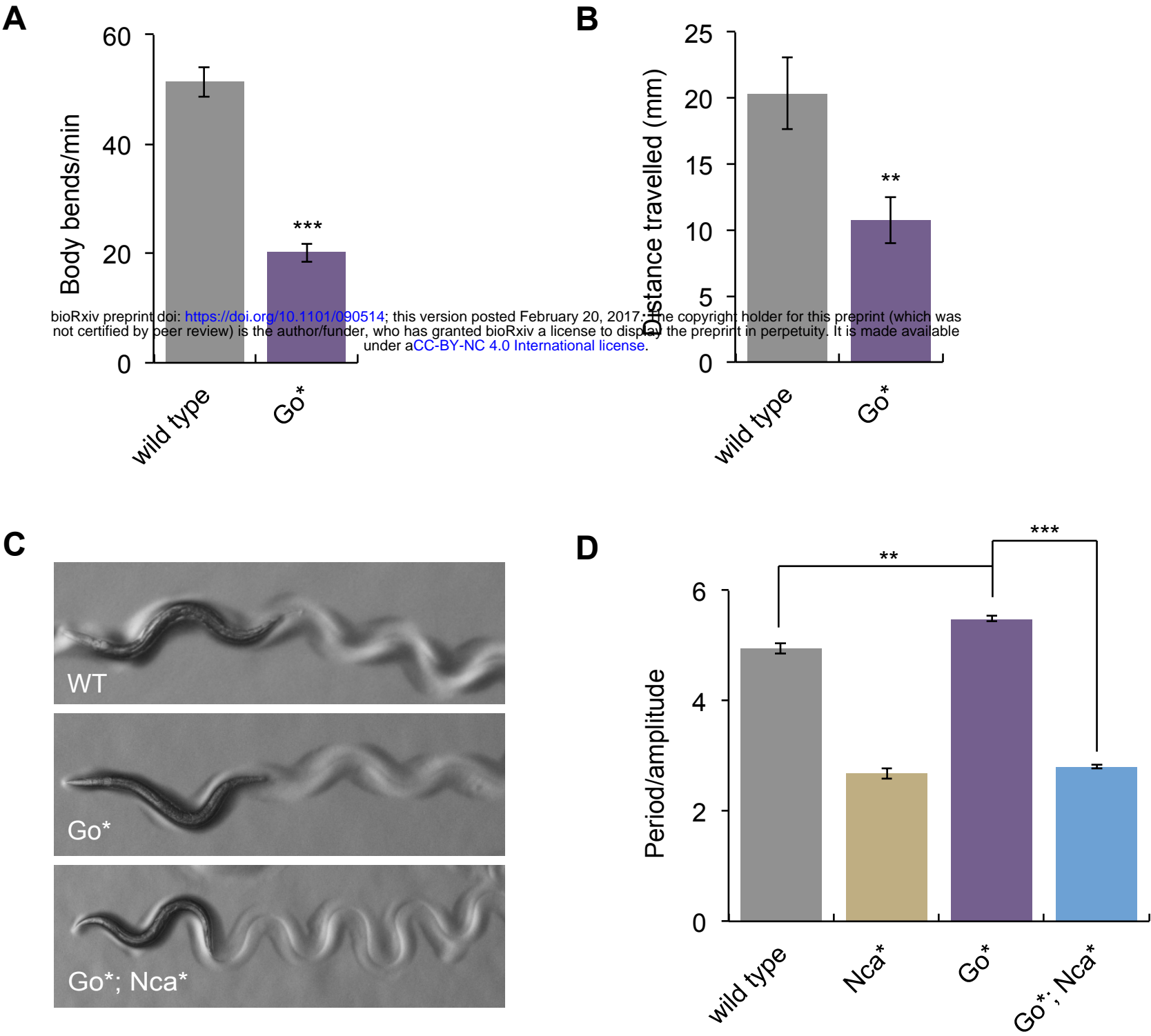


Figure 9



bioRxiv preprint doi: <https://doi.org/10.1101/090514>; this version posted February 20, 2017. The copyright holder for this preprint (which was not certified by peer review) is the author/funder, who has granted bioRxiv a license to display the preprint in perpetuity. It is made available under aCC-BY-NC 4.0 International license.

Figure 10

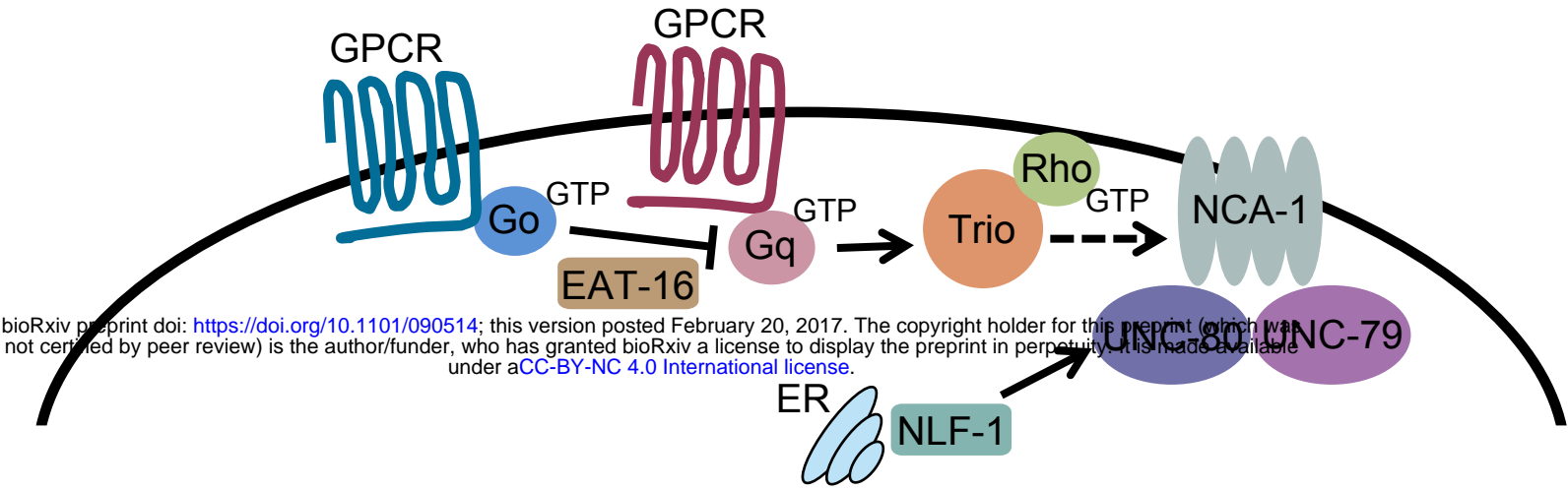
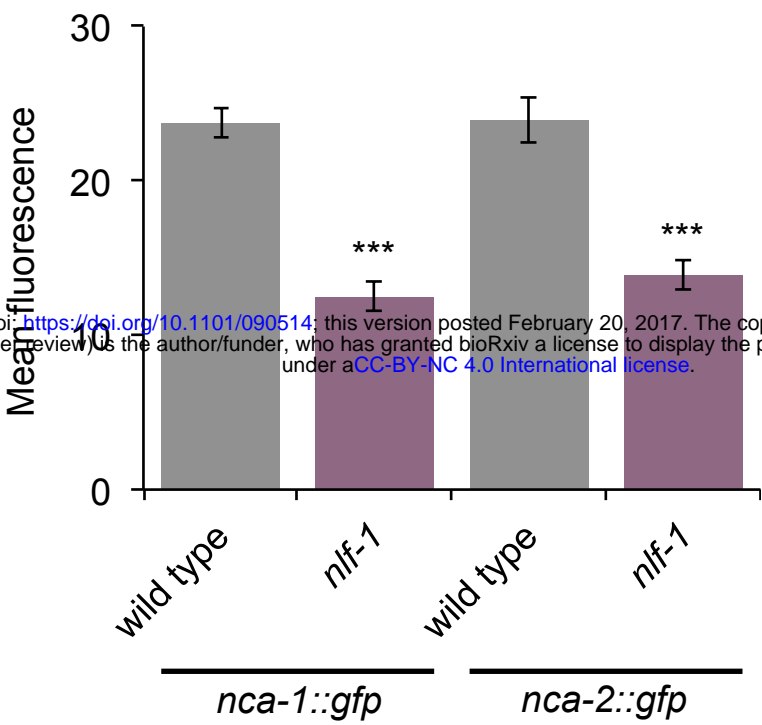


Figure S1



bioRxiv preprint doi: <https://doi.org/10.1101/090514>; this version posted February 20, 2017. The copyright holder for this preprint (which was not certified by peer review) is the author/funder, who has granted bioRxiv a license to display the preprint in perpetuity. It is made available under aCC-BY-NC 4.0 International license.

Table S1. List of strains

CB4856 Hawaiian wild isolate
EG303 *goa-1(n499 ox303)* I
EG304 *goa-1(n499 ox304)* I
EG327 *nlf-1(ox327)* X
EG330 *unc-80(ox330)* V
EG352 *nca-1(ox352)* IV
EG3447 *egl-30(tg26)* I *goa-1(n499)* I / *egl-30(tg26)* I *goa-1(+)* I
EG3498 *egl-30(tg26)* I *goa-1(n499)* I / *egl-30(tg26)* I *unc-13(e51)* I *gld-1(q126)* I
EG3532 *unc-13(n2813)* I ; *unc-80(ox301)* V
EG3647 *egl-30(tg26)* I ; *nlf-1(ox327)* X
EG3649 *egl-30(tg26)* I ; *unc-80(ox329)* V
EG3650 *egl-30(tg26)* I ; *unc-80(ox330)* V
EG3761 *unc-79(e1068)* III
EG3771 *egl-30(tg26)* I ; *unc-80(e1272)* V
EG3776 *egl-30(tg26)* I *unc-73(ox317)* I
EG3798 *egl-30(tg26)* I ; *egl-8(ox333)* V
EG3804 *nca-2(gk5)* III ; *nca-1(gk9)* IV
EG4036 *egl-30(tg26)* I ; *nca-2(gk5)* III ; *nca-1(gk9)* IV
EG4067 *goa-1(n499 ox304)* I ; *nca-1(ox352)* IV
EG4494 *nca-1(ox352)* IV ; *nlf-1(ox327)* X
EG4530 *nzls29[unc-17p::rho-1(G14V), unc-122p::gfp]* II ; *unc-79(e1068)* III
EG4531 *nzls29[unc-17p::rho-1(G14V), unc-122p::gfp]* II ; *unc-80(ox330)* V
EG4532 *egl-30(tg26)* I
EG4681 *nzls29[unc-17p::rho-1(G14V), unc-122p::gfp]* II ; *nlf-1(ox327)* X
EG4684 *nzls1[hs::rho-1(G14V), ttx-3p::gfp]* I ; *unc-79(e1068)* III
EG4685 *nzls1[hs::rho-1(G14V), ttx-3p::gfp]* I ; *unc-80(ox330)* V
EG4686 *nzls1[hs::rho-1(G14V), ttx-3p::gfp]* I ; *nlf-1(ox327)* X
EG4690 *nzls29[unc-17p::rho-1(G14V), unc-122p::gfp]* II ; *nca-2(gk5)* III ; *nca-1(gk9)* IV
EG4694 *unc-80(ox330)* V ; *nlf-1(ox327)* X
EG4697 *unc-79(e1068)* III ; *nlf-1(ox327)* X
EG4700 *nzls29[unc-17p::rho-1(G14V), unc-122p::gfp]* II ; *nca-1(gk9)* IV
EG4718 *nlf-1(ox327)* X ; *oxEx1041[cosmid F55A4, unc-17p::mCherry::H2B, lin-15(+)]*
EG4733 *nca-1(gk9)* IV ; *vals46[NCA-1::GFP, lin-15+]* X
EG4761 *nzls29[unc-17p::rho-1(G14V), unc-122p::gfp]* II ; *nca-2(gk5)* III
EG4782 *nzls29[unc-17p::rho-1(G14V), unc-122p::gfp]* II
EG4783 *nca-2(gk5)* III ; *vals41[NCA-2::GFP, lin-15+]*
EG4785 *egl-30(tg26)* I ; *nca-1(gk9)* IV
EG4786 *egl-30(tg26)* I ; *nca-2(gk5)* III
EG4834 *nca-1(gk9)* IV ; *nlf-1(ox327)* X
EG4835 *nca-2(gk5)* IV ; *nlf-1(ox327)* X
EG4836 *nlf-1(ox327)* X ; *vals46[NCA-1::GFP, lin-15+]*
EG4837 *nlf-1(ox327)* X ; *vals41[NCA-2::GFP, lin-15+]*
EG4943 *nlf-1(ox327)* X ; *oxEx1146[rab-3p::nlf-1(+) cDNA::GFP, myo-2p::mCherry]*
EG5217 *oxls412[rab-3p-FRT-mCherry-FRT-GFP-C3T, lin-15(+), hsp-FLP]* II
EG5218 *oxls414[unc-17p-FRT-mCherry-FRT-GFP-C3T, lin-15(+), hsp-FLP]* II
EG5252 *egl-30(tg26)* I ; *oxls412[rab-3p-FRT-mCherry-FRT-GFP-C3T, lin-15(+), hsp-FLP]* II
EG5263 *egl-30(tg26)* I ; *oxls414[unc-17p-FRT-mCherry-FRT-GFP-C3T, lin-15(+), hsp-FLP]* II
EG5279 *oxls434[unc-17Hp-FRT-mCherry-FRT-GFP-C3T, lin-15(+), hsp-FLP]* X
EG5287 *egl-30(tg26)* I ; *oxls434[unc-17Hp-FRT-mCherry-FRT-GFP-C3T, lin-15(+), hsp-FLP]* X
EG5320 *oxls435[unc-17βp-FRT-mCherry-FRT-GFP-C3T, lin-15(+), hsp-FLP]* II

EG5504 *nlf-1(tm3631)* X
EG5609 *egl-30(tg26)* I ; *rund-1(tm3622)* X
EG5611 *egl-30(tg26)* I ; *nlf-1(tm3631)* X
EG7249 *eri-1(mg366)* IV ; *lin-15(n744)* X
MT1102 *goa-1(n499)* I / +
N2 Bristol isolate, standard lab wild type
QT47 *nzIs1[hs::rho-1(G14V), ttx-3p::gfp]* I
VC9 *nca-2(gk5)* III
VC12 *nca-1(gk9)* IV
XZ1080 *egl-30(tg26)* I ; *unc-80(yak8)* V
XZ1113 *egl-30(tg26)* I ; *unc-80(yak35)* V
XZ1114 *egl-30(tg26)* I ; *unc-80(yak36)* V
XZ1115 *egl-30(tg26)* I ; *unc-79(yak37)* III
XZ1151 *egl-30(tg26)* I
XZ1152 *egl-30(tg26)* I ; *nuls183[unc-129p::NLP-21-Venus, myo-2p::NLS-GFP]* III
XZ1186 *egl-30(tg26)* I ; *nuls183[unc-129p::NLP-21-Venus, myo-2p::NLS-GFP]* III; *unc-80(yak56)* V
XZ1191 *egl-30(tg26)* I ; *unc-79(yak61)* III *nuls183[unc-129p::NLP-21-Venus, myo-2p::NLS-GFP]* III
XZ1229 *egl-30(tg26)* I ; *unc-79(yak73)* III *nuls183[unc-129p::NLP-21-Venus, myo-2p::NLS-GFP]* III
XZ2008 *lin-15(n765ts)* X ; *oxEx1144[nlf-1p::GFP, lin-15(+)]*
XZ2009 *nlf-1(ox327)* X ; *oxEx1147[nlf-1p::nlf-1(+):GFP, myo-2p::mCherry]*
XZ2010 *nlf-1(ox327)* X ; *oxEx1149[unc-17p::nlf-1(+) cDNA::GFP, myo-2p::mCherry]*
XZ2011 *nlf-1(ox327)* X ; *oxEx1155[unc-17Hp::nlf-1(+) cDNA::GFP, myo-2p::mCherry]*
XZ2012 *nlf-1(ox327)* X ; *oxEx1151[acr-2p::nlf-1(+) cDNA::GFP, myo-2p::mCherry]*
XZ2013 *nlf-1(ox327)* X ; *oxEx1323[unc-17βp::nlf-1(+) cDNA::GFP, myo-2p::mCherry]*
XZ2014 *nlf-1(ox327)* X ; *oxEx1152[glr-1p::nlf-1(+) cDNA::GFP, myo-2p::mCherry]*

Table S2. List of plasmids

Miscellaneous plasmids

pCFJ90	<i>myo-2::mCherry</i>
pGH47	<i>unc-17p::mCherry::H2B</i>
pL15EK	<i>lin-15(+)</i>
pWD79-2RV	<i>hsp-16.48p::FLP</i>
QT#99	<i>Phs::GFP-C3T</i>
F55A4	cosmid carrying the <i>nlf-1</i> gene F55A4.2, used to make <i>oxEx1041</i> (10 ng/μl)
yk1279a1	<i>nlf-1</i> full length cDNA
Litmus 28i	
Litmus 38i	

Gateway entry clones

p_C06E1.4-93	<i>glr-1p</i> [4-1] (727 bp of the <i>glr-1</i> promoter upstream of and including the ATG)
pADA180	<i>unc-17Hp</i> [4-1] (derived from the <i>unc-17</i> promoter of pGH1, carrying a 127 bp deletion that removes the nerve cord β enhancer, expressed in head cholinergic neurons)
pCFJ31	<i>acr-2p</i> [4-1] (3362 bp of the <i>acr-2</i> promoter upstream of the ATG)
pCR110	<i>GFP</i> [1-2]
pCR185	<i>GFP::unc-54</i> 3'UTR [2-3]
pEntry[2-3]-UTR[unc-54]	<i>unc-54</i> 3'UTR [2-3]
pEntry[4-1]-P[rab-3]	<i>rab-3p</i> [4-1] (1224 bp of the <i>rab-3</i> promoter upstream of and including the ATG)
pGH1	<i>unc-17p</i> [4-1] (3229 bp of the <i>unc-17</i> promoter upstream of and including the ATG)
pMA1	<i>nlf-1p</i> [4-1] (5665 bp of the <i>nlf-1</i> promoter upstream of and including the ATG)
pMA2	<i>nlf-1(+)</i> gene with introns [1-2]
pMA3	<i>nlf-1</i> cDNA [1-2] (derived from yk1279a1)
pMA19	<i>C3T::unc-54</i> 3'UTR [2-3]
pMA23	<i>unc-17βp</i> [4-1] (a fusion of the <i>unc-17</i> nerve cord β enhancer to the minimal <i>unc-17</i> promoter consisting of the 382 bp upstream of and including the ATG, expressed in ventral nerve cord cholinergic neurons)
pWD178	<i>FRT::mCherry::let-858</i> 3'UTR:: <i>FRT::GFP</i> [1-2]

Gateway expression constructs

pMA4	<i>nlf-1p::GFP</i> , used to make <i>oxEx1144</i> (10 ng/μl)
pMA5	<i>rab-3p::nlf-1</i> cDNA:: <i>GFP</i> , used to make <i>oxEx1146</i> (10 ng/μl)
pMA6	<i>nlf-1p::nlf-1(+)</i> :: <i>GFP</i> , used to make <i>oxEx1147</i> (10 ng/μl)
pMA8	<i>unc-17p::nlf-1</i> cDNA:: <i>GFP</i> , used to make <i>oxEx1149</i> (10 ng/μl)
pMA9	<i>acr-2p::nlf-1</i> cDNA:: <i>GFP</i> , used to make <i>oxEx1151</i> (10 ng/μl)
pMA10	<i>glr-1p::nlf-1</i> cDNA:: <i>GFP</i> , used to make <i>oxEx1152</i> (10 ng/μl)
pMA11	<i>unc-17Hp::nlf-1</i> cDNA:: <i>GFP</i> , used to make <i>oxEx1155</i> (10 ng/μl)
pMA27	<i>rab-3p::FRT::mCherry::let-858</i> 3'UTR:: <i>FRT::GFP::C3T::unc-54</i> 3'UTR, used to make <i>oxls412</i> (10 ng/μl)
pMA28	<i>unc-17p::FRT::mCherry::let-858</i> 3'UTR:: <i>FRT::GFP::C3T::unc-54</i> 3'UTR, used to make <i>oxls414</i> (10 ng/μl)
pMA39	<i>unc-17Hp::FRT::mCherry::let-858</i> 3'UTR:: <i>FRT::GFP::C3T::unc-54</i> 3'UTR, used to make <i>oxls434</i> (10 ng/μl)
pMA40	<i>unc-17βp::FRT::mCherry::let-858</i> 3'UTR:: <i>FRT::GFP::C3T::unc-54</i> 3'UTR, used to make <i>oxls435</i> (10 ng/μl)
pMA52	<i>unc-17β::nlf-1</i> cDNA:: <i>GFP</i> , used to make <i>oxEx1323</i> (10 ng/μl)